Competition between deformability and charge transport in semiconducting polymers for flexible and stretchable electronics

Adam D. Printz and Darren J. Lipomi

Citation: Applied Physics Reviews **3**, 021302 (2016); doi: 10.1063/1.4947428
View online: http://dx.doi.org/10.1063/1.4947428
View Table of Contents: http://scitation.aip.org/content/aip/journal/apr2/3/2?ver=pdfcov
Published by the AIP Publishing

APPLIED PHYSICS REVIEWS

Competition between deformability and charge transport in semiconducting polymers for flexible and stretchable electronics

Adam D. Printz and Darren J. Lipomi[a)]
Department of NanoEngineering, University of California, San Diego, 9500 Gilman Drive, Mail Code 0448, La Jolla, California 92093-0448, USA

(Received 10 March 2016; accepted 11 April 2016; published online 28 April 2016)

The primary goal of the field concerned with organic semiconductors is to produce devices with performance approaching that of silicon electronics, but with the deformability—flexibility and stretchability—of conventional plastics. However, an inherent competition between deformability and charge transport has long been observed in these materials, and achieving the extreme (or even moderate) deformability implied by the word "plastic" concurrently with high charge transport may be elusive. This competition arises because the properties needed for high carrier mobilities—e.g., rigid chains in π-conjugated polymers and high degrees of crystallinity in the solid state—are antithetical to deformability. On the device scale, this competition can lead to low-performance yet mechanically robust devices, or high-performance devices that fail catastrophically (e.g., cracking, cohesive failure, and delamination) under strain. There are, however, some observations that contradict the notion of the mutual exclusivity of electronic and mechanical performances. These observations suggest that this problem may not be a fundamental trade-off, but rather an inconvenience that may be negotiated by a logical selection of materials and processing conditions. For example, the selection of the poly(3-alkylthiophene) with a critical side-chain length—poly(3-heptylthiophene) ($n = 7$)—marries the high deformability of poly(3-octylthiophene) ($n = 8$) with the high electronic performance (as manifested in photovoltaic efficiency) of poly(3-hexylthiophene) ($n = 6$). This review explores the relationship between deformability and charge transport in organic semiconductors. The principal conclusions are that reducing the competition between these two parameters is in fact possible, with two demonstrated routes being: (1) incorporation of softer, insulating material into a stiffer, semiconducting material and (2) increasing disorder in a highly ordered film, but not enough to disrupt charge transport pathways. The aim of this review is to provide a bridge between the fields interested in electronic properties and mechanical properties of conjugated polymers. We provide a high-level introduction to some of the important electronic and mechanical properties and measurement techniques for organic electronic devices, demonstrate an apparent competition between good electronic performance and mechanical deformability, and highlight potential strategies for overcoming this undesirable competition. A marriage of these two fields would allow for rational design of materials for applications requiring large-area, low-cost, printable devices that are ultra-flexible or stretchable, such as organic photovoltaic devices and wearable, conformable, or implantable sensors. *Published by AIP Publishing.*
[http://dx.doi.org/10.1063/1.4947428]

TABLE OF CONTENTS

[a)]Author to whom correspondence should be addressed. Electronic mail: dlipomi@ucsd.edu.

I. INTRODUCTION

Organic semiconductors have recently exhibited hole mobilities over 40 $cm^2\ V^{-1}\ s^{-1}$ in organic field-effect transistors (OFETs)[1] and power conversion efficiencies (*PCE*) over 10% in organic photovoltaic (OPV) devices.[2–4] These materials also promise high flexibility and intrinsic stretchability, which allow for many applications previously impossible (or much more expensive) with stiffer inorganic materials.[5–8] Inorganic materials can be patterned to allow for stretchability (e.g., by introducing sinusoidal buckles),[9–11] but in applications where high electronic performance is not required, using organic materials with intrinsic stretchability and the ability to be tailored on the molecular scale could simplify processes of fabrication and increase functionality.[12–14] However, there is an apparent competition between good electronic performance—as manifested in charge-carrier mobility and photovoltaic efficiency—and desirable mechanical properties such as high deformability and elastic range.[7,15–17] Overcoming this apparent competition and coupling good electronic performance and deformability into a single material would facilitate high performance, yet low-cost,[18–20] printable,[21–25] wearable,[26,27] and mechanically robust devices.[28,29] It is therefore important to understand what parameters affect these properties and determine if it is indeed possible to co-optimize them. Control over molecular ordering is frequently used to manipulate film properties and parameters that have been studied to this end include the rigidity of the polymer backbone,[30,31] the length and branching of the solubilizing side-chains (required because unsubstituted conjugated polymers are insoluble in common solvents),[7,13,32–34] processing conditions such as solvent evaporation rate[16] and annealing,[35–39] and molecular orientation.[40–45]

Much of the work in the field concerned with organic electronics has been focused on improving device performance; high deformability and elastic range are often assumed to be intrinsic to polymer semiconductors, and therefore mechanical properties are frequently left unstudied for many materials. However, the electronic *and* mechanical properties of some conjugated polymers have been investigated (Figure 1). Among all conjugated polymers, the most studied family in the literature is poly(3-alkylthiophene)s (P3ATs), which have been the subject of experiments including the effects of molecular weight,[46–51] processing conditions including casting solvent,[52,53] film thickness,[54] film morphology,[55,56] alkyl side-chain length,[38,57,58] and regioregularity.[59] Poly(3-alkylthiophenes) are simple model systems because they comprise a repeat unit of a thiophene with a single alkyl side-chain, but they suffer from low hole mobilities ($<1\ cm^2\ V^{-1}\ s^{-1}$) and have a bandgap on the order of 2 eV.[60] Polymers with narrow bandgaps, such as those based on alternating electron-rich and electron-poor subunits (several of which are shown in Figure 1),[41,61–65] are of particular interest in organic photovoltaics because they can absorb light at longer wavelengths (and therefore better overlap with the solar spectrum), which ideally leads to improved photovoltaic performance over P3ATs.[61] These low-bandgap materials can also exhibit higher hole mobilities, above 12 $cm^2\ V^{-1}\ s^{-1}$ in OFETs.[62] Another component critical to organic electronics—at least in OPVs—is fullerene derivatives, such as $PC_{61}BM$ and $PC_{71}BM$ (Figure 1), which are commonly blended with polymers and act as electron acceptors in photovoltaic devices, and although they are not semiconducting polymers, no discussion on organic electronics is complete without addressing them. They have high embodied energy and behave as anti-plasticizers for semiconducting polymers;[20,66] this property leads to low deformability[66] as well as poorer adhesion and cohesion of layers.[67,68] The high cost and poor mechanical properties of fullerenes have thus led many researchers to explore replacing fullerenes with electron acceptors based on small molecules[69] or polymers,[70–72] and all-conjugated block copolymers containing both electron-donating (e.g., poly(3-hexylthiophene) (P3HT)) and electron-accepting (e.g., poly-((9,9-dioctylfluorene)-2,7-diyl-alt-[4,7-bis(thiophen-5-yl)-2,1,3-benzothiadiazole]-2′,2″-diyl) (PFTBT)) blocks (Figure 1).[73]

The primary aim of this review is to bridge the knowledge of the fields interested in electronic properties and mechanical properties of organic semiconductors. We do this with the hope that researchers will focus on the likely applications for organic semiconductors: printable, wearable, and implantable devices, which require not only good electronic performance but also mechanical robustness and frequently high deformability as well. In Sections II and III, we have included brief introductions to the measurement of electronic and mechanical properties relevant in organic electronic devices. Experts in the field of charge transport can safely skip Section II, while experts in the field of mechanical properties can safely skip Section III. Due to the limited literature on the mechanical properties of small molecules, the scope of this review is focused on polymers and also, because of their relevance to organic photovoltaics, polymer:fullerene composites.

II. CHARGE TRANSPORT IN ORGANIC SEMICONDUCTORS

In organic semiconductors, the alternating single and double bonds between carbon atoms give rise to molecular conjugation—the overlap of p-orbitals across the single bonds—and result in the delocalization of π-electrons and the opening up of a bandgap. In general, electronic performance in organic semiconductors depends on their solid-state packing structure.[74] Packing dictates intermolecular electronic coupling (which is determined by the wavefunction overlap, partially determined by π-π stacking) and thus the charge transport.[74] Aggregates and crystallites typically have a smaller π-π stacking distance than amorphous polymer and therefore tend to have higher mobilities.[75] While these aggregates and crystallites are frequently required for high electronic performance, they are generally stiffer than disordered amorphous polymer and therefore tend to decrease deformability of films. Aggregates of planar polymers and small molecules such as P3HT generally exhibit an anisotropy in mobility along three axes. In Figure 2, the a-axis is the lamellar stacking axis and it is the direction of the slowest charge transport. The b-axis is the π-π stacking axis and has relatively fast charge transport. The c-axis is along the conjugated backbone and because of

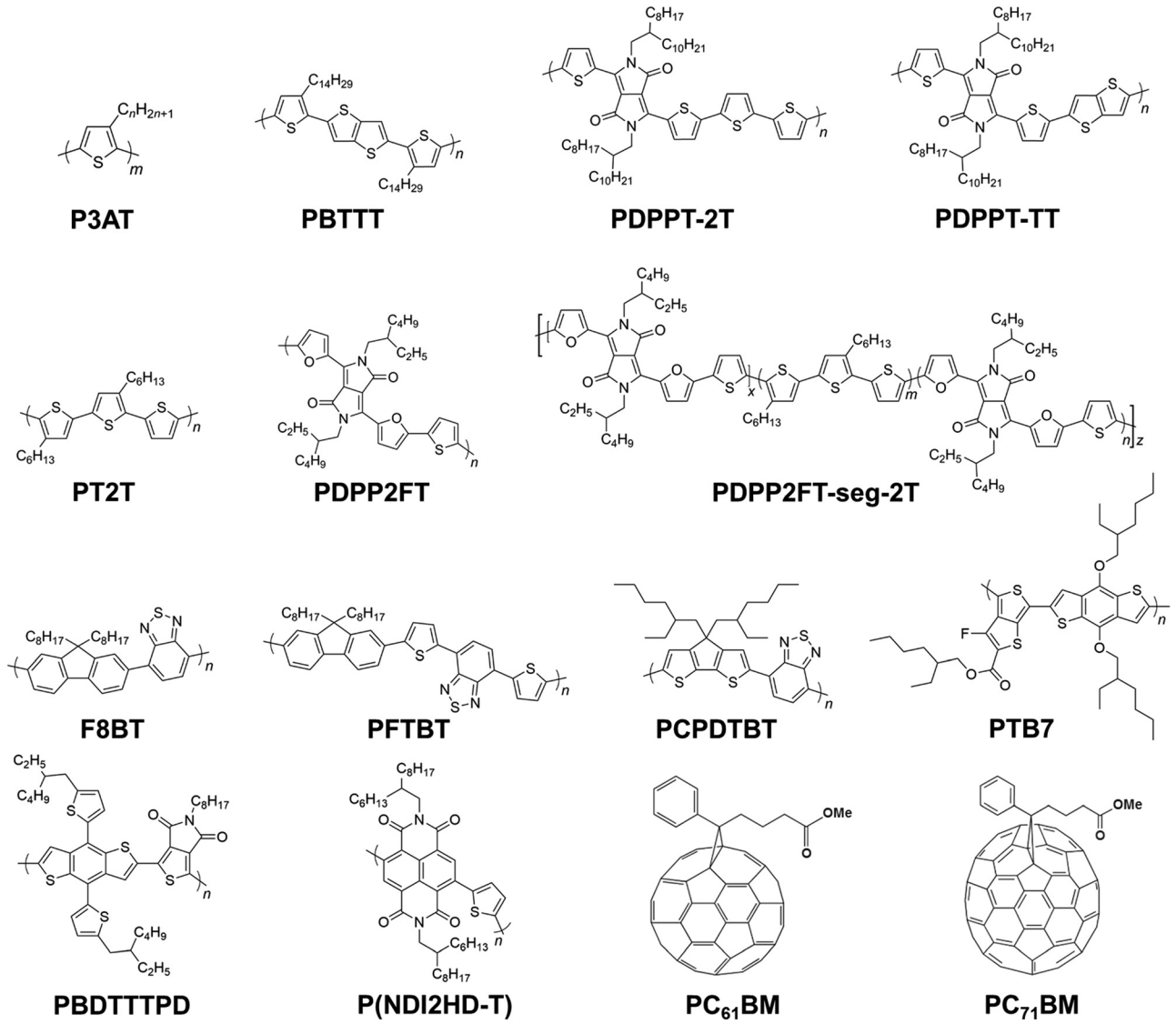

FIG. 1. Molecular structures of the organic semiconductors discussed in this review.

the covalently linked conjugated units, charge transport is highest in this direction.[75–77]

Transfer of charge through a film requires a percolated network of conjugation, usually through well-ordered polymer aggregates (whose presence in some materials is correlated with stiffness and brittleness).[75,78,79] Aggregates are often required for charge transport because of their greater degree of conjugation when compared with disordered or completely amorphous regions, where kinks can occur and disrupt the planarity of the molecule.[79,80] This disruption of planarity results in a breaking of conjugation, essentially creating a dead-end (along that polymer chain) for charges and forcing them to hop to a new chain (or another part of the same chain).[79] For charges, chain-hopping is a much slower process than proceeding along a single chain and causes a reduction in mobility; chain-hopping mobility is limited to $\sim 0.1\,\mathrm{cm}^2\ \mathrm{V}^{-1}\ \mathrm{s}^{-1}$, several orders of magnitude less than the highest performance organic semiconductors.[75,79,81] An additional reason for charges to be transported predominantly through aggregates (at least in semicrystalline films) is related to the respective bandgaps of polymer in aggregated regions compared with that of polymer in amorphous regions. The band gap is inversely correlated with the conjugation length of the polymer chains; in amorphous regions, the conjugation length of polymer chains is much shorter than in aggregates, and thus there is an energy barrier that inhibits transferring charge from aggregates to amorphous regions.[75] In semicrystalline polymers, these two effects present an interesting problem: at the boundary of each aggregate is disordered or amorphous polymer,[82] and if the planarity of these molecules is disrupted, hopping must occur and the charge-carrier mobility is thus limited.[81] However, despite these potential bottlenecks, semicrystalline films exhibiting high mobility do in fact exist.[1,62] Salleo and coworkers put forth the hypothesis that in high-mobility semicrystalline films, the disordered regions are bypassed by polymer chains without kinks (i.e., tie-chains or tie-molecules) that connect aggregates to each other and allow charge to be transported efficiently from aggregate to aggregate.[75,79] In Sections II A–II C, we will briefly introduce the device physics of OFETs and OPVs, as well as ordering in thin films.

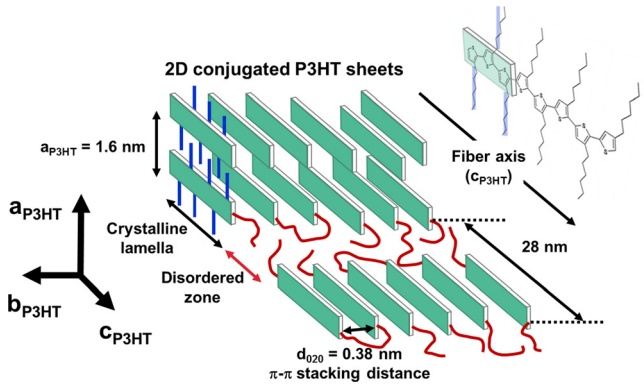

FIG. 2. The stacking structure of P3HT. The charge mobility is highest along the fiber axis or backbone (c_{P3HT}) and lower in the π-π stacking direction (b_{P3HT}). Negligible transport occurs in the a_{P3HT} direction. Reproduced with permission from M. Brinkmann, J. Polym. Sci., Part B: Polym. Phys. **49**, 1218–1233 (2011). Copyright 2011 Wiley-VCH Verlag GmbH & Co. KGaA.

A. Device physics: Organic field-effect transistors

In OFETs, current is controlled by voltage and is dependent on the carrier mobility in the semiconducting layer. There are three general classes of transistors: p-channel, n-channel, and ambipolar. The charge carriers are holes in p-channel transistors and electrons in n-channel transistors, while the charge carriers can be either holes or electrons depending on operating parameters—that is, the source-drain and source-gate voltages—in ambipolar transistors. OFETs tend to be p-channel transistors if the Fermi level, E_F, of the source and drain contacts is closer to the highest occupied molecular orbital (HOMO) of the semiconductor than to its lowest unoccupied molecular orbital (LUMO). If instead, E_F of the source/drain contacts is closer to the semiconductor LUMO than its HOMO, the OFET will exhibit n-channel behavior.[83] OFETs can have many different architectures, but typically they comprise a source (or charge-injecting) electrode and drain (or charge-extracting) electrode lying in the same plane, a semiconductor layer filling the channel between the source and drain, a gate dielectric layer atop or below the semiconductor, and a gate electrode in contact with the dielectric layer (but not the semiconductor). An example of a bottom-gate coplanar OFET is shown in Figure 3(a).

Briefly, transistors operate in the following manner. A voltage is applied between the source and the gate electrodes, V_G, which causes a mobile layer of charge to form in the semiconductor at the interface with the dielectric layer. The number of mobile charges is proportional to the capacitance of the dielectric, C_d, and the gate voltage. However, before the induced charges can become mobile, there are deep trap states that must be filled; the bias required to fill these trap states is the threshold voltage, V_{Th}. The number of mobile charge carriers is thus proportional to the effective voltage, $V_G - V_{Th}$, rather than just V_G. In the case of p-channel transistors—e.g., semiconductor layers of P3HT or poly(2,5-bis(3-alkylthiophen-2-yl)thieno[3,2,-*b*]-thiophene (PBTTT)—V_G is much lower than 0 V and the HOMO and LUMO bands of the semiconductor bend up, resulting in the accumulation of holes at the semiconductor/dielectric interface (Figure 3(b), **left**). In n-channel transistors—e.g., semiconductor layers of poly(9,9-dioctylfluorene-alt-benzothiadiazole) (F8BT, Figure 1)[84]—V_G is greater than 0 V and the HOMO and LUMO bands of the semiconductor bend down, resulting in the accumulation of electrons at the semiconductor/dielectric interface (Figure 3(b), **right**). In p-channel transistors, the energy barrier between the HOMO of the semiconductor and the Fermi energy level (E_F) of the source and drain must be as small as possible, or in other words, the ionization potential (IP) of the semiconductor should be similar to the work function of the source and drain. In n-channel transistors, it is instead desirable for the energy barrier between the LUMO (rather than the HOMO) and the E_F of the source and drain to be small as possible, that is, the electron affinity (EA) of the semiconductor should be similar to the work function of the source and drain. An additional voltage is applied between the source and drain, V_{DS}, which offsets the energy levels of the source and drain and bends the HOMO and LUMO levels of the semiconductor (Figure 3(c)). When $0 < V_{DS} \ll V_G$, a linear gradient of charge density occurs from the source to drain. The potential at the source is 0 and increases linearly through the channel until it reaches V_{DS} at the drain. The current flowing through the channel from source to drain, I_{DS}, is proportional to V_{DS} in this "linear regime." If V_{DS} is increased to the point where it is equal to $V_G - V_{Th}$, the channel becomes "pinched off" at the drain because the difference between the local potential and the gate voltage is below the threshold voltage.[85] A depletion region results and its high electric field allows current to be swept across to the drain at a saturation current $I_{DS,sat}$. As V_{DS} is increased further, there is no (substantial) increase in current, and instead the depletion region expands and the channel becomes slightly shorter. This regime, where the current remains constant as V_{DS} is increased, is the "saturation regime."

Typically, OFET data are plotted as the source-drain current versus the source-drain voltage—i.e., the output plot—or the source-drain current versus the gate voltage—i.e., the transfer plot. In the output plot (Figure 4(a)), the source-drain current initially increases with the source-drain voltage linearly (the linear regime). In the linear regime, when $V_{DS} \ll V_G$ (Figure 4(b)), the field-effect mobility, μ_{lin}, can be extracted from the linear fit of the slope of I_{DS} vs. V_G using the following equation:

$$I_{DS} = \mu_{lin} C_d \frac{W}{L}(V_G - V_{Th})V_{DS}, \quad (1)$$

where W and L are the semiconductor channel width and length, respectively. The onset voltage, V_{on}, or the voltage at which I_{DS} increases quickly can be found in the log(I_{DS}) vs. V_G plot (Figure 4(b)). In the saturation regime, $V_{DS} > V_G - V_{Th}$ (Figure 4(c)), the field-effect mobility, μ_{sat}, can be extracted from the slope of the linear fit in the saturation regime on the plot of $(I_{DS,sat})^{1/2}$ vs. V_G, and the threshold voltage, V_{Th}, can be extracted from the interception of the linear fit and the x-axis using the following equation:[86,87]

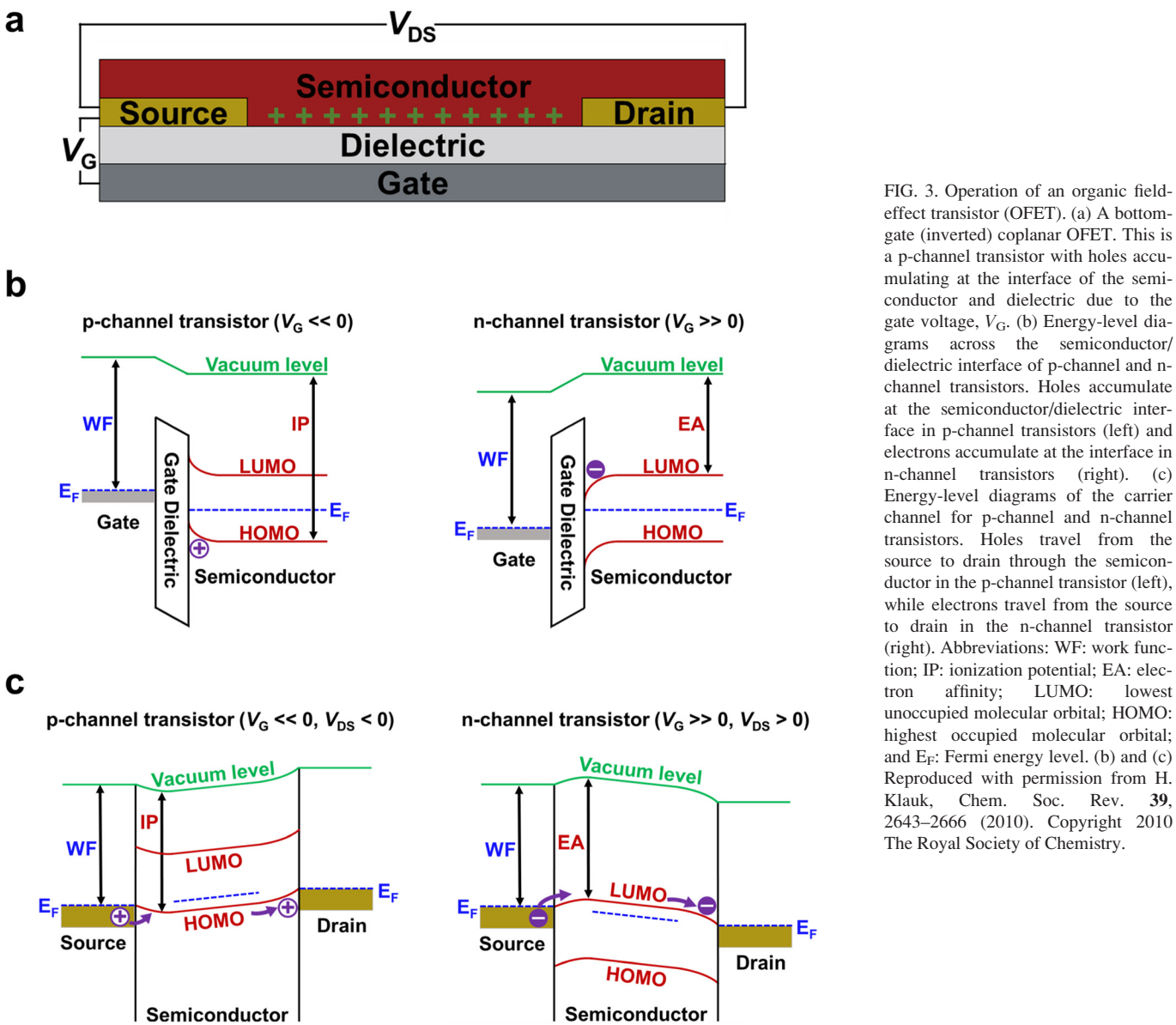

FIG. 3. Operation of an organic field-effect transistor (OFET). (a) A bottom-gate (inverted) coplanar OFET. This is a p-channel transistor with holes accumulating at the interface of the semiconductor and dielectric due to the gate voltage, V_G. (b) Energy-level diagrams across the semiconductor/dielectric interface of p-channel and n-channel transistors. Holes accumulate at the semiconductor/dielectric interface in p-channel transistors (left) and electrons accumulate at the interface in n-channel transistors (right). (c) Energy-level diagrams of the carrier channel for p-channel and n-channel transistors. Holes travel from the source to drain through the semiconductor in the p-channel transistor (left), while electrons travel from the source to drain in the n-channel transistor (right). Abbreviations: WF: work function; IP: ionization potential; EA: electron affinity; LUMO: lowest unoccupied molecular orbital; HOMO: highest occupied molecular orbital; and E_F: Fermi energy level. (b) and (c) Reproduced with permission from H. Klauk, Chem. Soc. Rev. **39**, 2643–2666 (2010). Copyright 2010 The Royal Society of Chemistry.

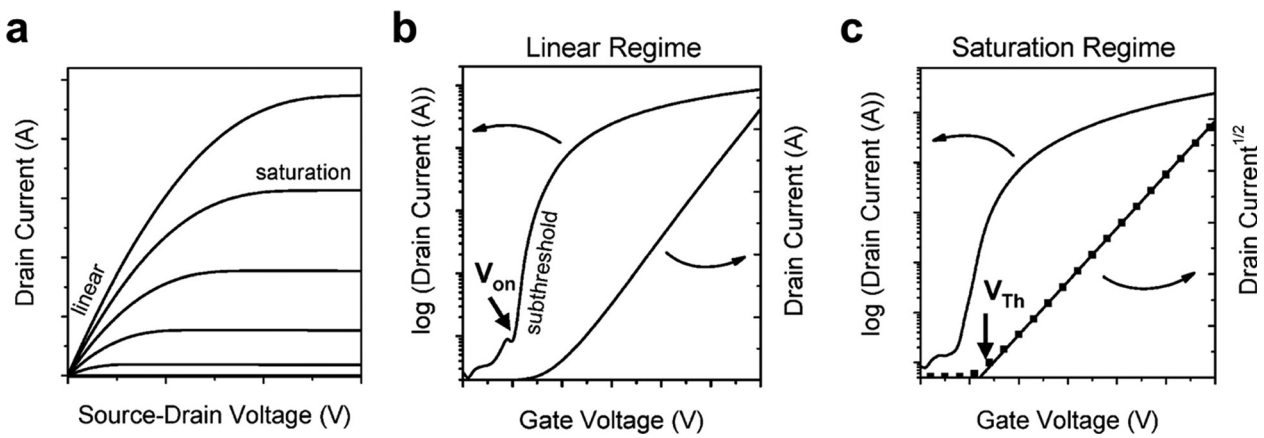

FIG. 4. Hypothetical output and transfer plots for an OFET. (a) Output plot of the source-drain current versus the source-drain voltage. (b) Transfer plot of the source-drain current versus the gate voltage for a typical OFET in the linear regime. (c) Transfer plot of the source-drain current versus the gate voltage for a typical OFET in the saturation regime. Reproduced with permission from J. Zaumseil and H. Sirringhaus, Chem. Rev. **107**, 1296–1323 (2007). Copyright 2007 American Chemical Society.

$$I_{DS,sat} = \mu_{sat} C_d \frac{W}{2L} (V_G - V_{Th})^2. \quad (2)$$

In addition to charge-carrier mobility, the other important material parameter for OFETs is the on/off ratio, which is the ratio of the maximum drain current in the "on" state of the transistor to the minimum drain current in the "off" state of the transistor. A high on/off ratio is desirable since it is essentially the signal-to-noise ratio for a transistor.

B. Device physics: Organic photovoltaics

Charge transport in OPV devices manifests principally in the short-circuit current and fill factor (FF) (and thus in the power conversion efficiency). Typically, the device architecture of OPVs is a stack comprising an electrode, an active layer consisting of an intimately mixed electron donating material with an electron accepting material—known as a bulk heterojunction (BHJ)—and a transparent electrode (Figure 5(a)). Depending on the molecular components, the bulk heterojunction can take on many different morphologies. For polymer-fullerene bulk heterojunctions, these morphologies include a molecularly mixed amorphous composite, a ternary blend with pure or enriched phases separated by mixed phases, or a well ordered blend with bimolecular crystallization (Figure 5(a)).[88] The operation of OPVs is detailed in Figure 5(b). In step (1), light is absorbed by the BHJ—in this example by the electron donor—and it excites an electron from the HOMO to the LUMO. Upon excitation of the electron to the LUMO, there in an absence of an electron in the HOMO level (a hole). This electron-hole pair (exciton) is tightly bound because of the relatively low dielectric constant of organic photovoltaics. (In inorganic devices, the dielectric constant is higher and effectively screens the charges of the electron and hole, allowing them to separate and diffuse through the device.[89]) (2) Excitons diffuse through the film until they reach an interface of the electron donor and acceptor, or until they recombine. Exciton diffusion lengths for organic semiconductors are typically reported to be less than 20 nm, so ideally donor and acceptor phases will be sufficiently small to allow for excitons to diffuse to interfaces before they have the opportunity to recombine.[90] (3) In the case where an interface is reached, if the energetics are favorable, the electron will transfer to the electron acceptor; the exciton binding energy is ~0.3–0.5 eV, so an offset of the LUMOs of the donor and the acceptor of at least 0.3 eV is usually required to allow for charge separation.[89] (4) and (5) Once the charges separate at the donor/acceptor interface, the electrons will drift through the acceptor toward the cathode (the electrode with the relatively lower work function), and the holes will drift through the donor toward the anode (the electrode with the relatively higher work function).

Device measurements are made by sweeping the electrode voltage, V, and plotting it against the current density, J. A hypothetical J-V curve of an OPV device is shown in Figure 6. The points of interest are the short-circuit current density, J_{SC}, which is the current density when the device is at zero voltage, the open-circuit voltage, V_{OC}, which is the

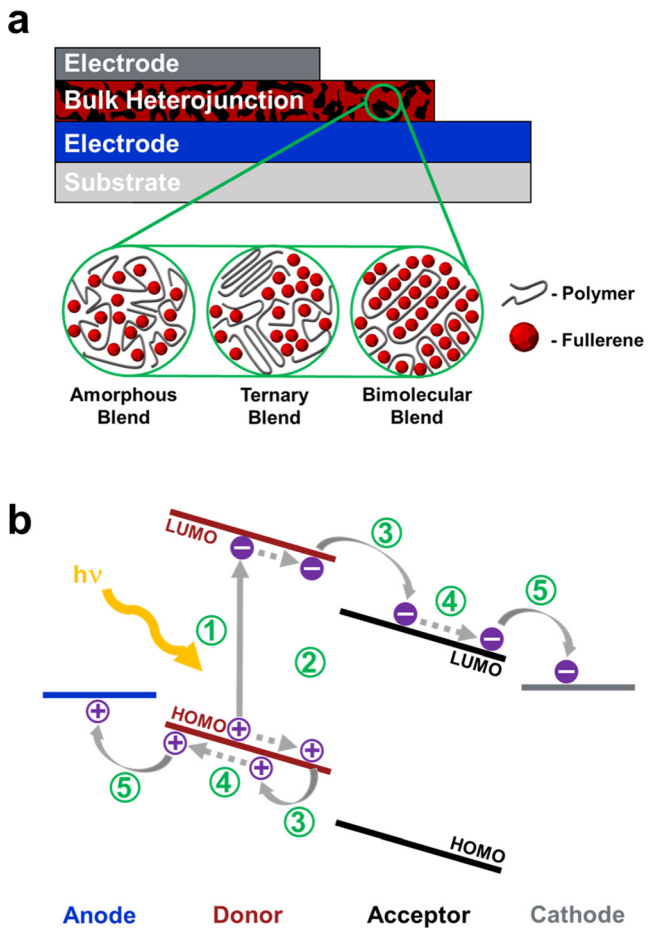

FIG. 5. Schematic drawing and operation of OPV devices. (a) A conventional OPV architecture with a polymer:fullerene bulk heterojunction (BHJ) active layer. The three archetypal morphologies of the BHJ are highlighted: an amorphous blend of electron donor and acceptor; a ternary blend with pure or enriched phases of donor or acceptor surrounded by disordered blends of the two; and an intimately mixed bimolecular blend, with the fullerene aligning along the chains of the polymer. (b) Hypothetical energy-level diagrams for the OPV device in (a). Light is absorbed and a tightly bound electron-hole pair (exciton) is created in step 1, followed by diffusion of the exciton to the donor/acceptor interface in step 2. The charges then separate with the electron jumping to the acceptor and the hole remaining in the donor (step 3). The charges then drift towards the electrodes (the holes toward the anode and the electrons toward the cathode, step 4) and then finally are transferred to the electrodes (step 5).

voltage when there is no current flowing, and the maximum power point, P_{max}, which is the point at which the product of the current density and voltage is at its maximum. The current density and voltage at P_{max} are J_{max} and V_{max}, respectively, and these can be used to determine the fill factor, FF, by the following equation:

$$FF = \frac{J_{max} V_{max}}{J_{SC} V_{OC}}. \quad (3)$$

The ideal J-V curve is a rectangle, and as the experimental curve becomes more rectangular (assuming J_{max} approaches J_{SC} and V_{max} approaches V_{OC}), the FF approaches unity. However, in practice, losses due to resistance in the electrodes and contacts (i.e., series resistance, R_{series}) and shunting due to defects in the film (represented by the shunt resistance, R_{shunt}) prevent a FF of unity. The power conversion

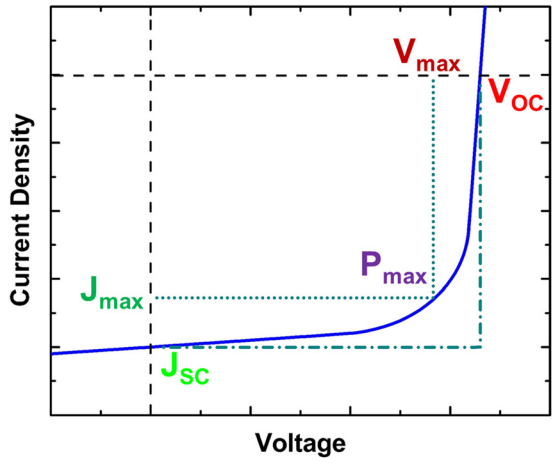

FIG. 6. Idealized *J-V* curve for an OPV device. The short-circuit current density, J_{SC}, is the current when the voltage across the cell is zero (the vertical dashed black lines), and the open-circuit voltage, V_{OC}, is the voltage when the current is zero (the horizontal dashed black line). J_{max} and V_{max} are the current density and voltage at the point of maximum power point, P_{max}. The fill-factor, *FF*, is the ratio of the rectangle created from the origin to J_{max} and V_{max} (dotted line) to the rectangle created from the origin to J_{SC} and V_{OC} (dashed-dotted line).

efficiency, which is the ratio of power output of the device to the power incident (the amount of power contributed by the sunlight), P_{inc} (100 mW cm^{-2} at AM 1.5G), can then be calculated by the following equation:

$$PCE = \frac{P_{max}}{P_{inc}} = \frac{J_{SC}V_{OC}FF}{P_{inc}}. \quad (4)$$

C. Order in thin-film organic semiconductors

X-ray diffraction (XRD) is often utilized to determine long-range ordering of organic semiconductor films, and improved ordering has been correlated to improve charge-carrier mobility in many different systems (but also to a reduction in compliance and ductility). For example, the hole mobility, μ_h, of poorly ordered regiorandom P3HT is several orders of magnitude lower than more ordered films of highly regioregular P3HT.[83] However, a high degree of ordering as determined by XRD is not always correlated with improved charge transport. Despite the favorable electronic peformance of Poly({4,8-bis[(2-ethylhexyl)oxy]benzo[1,2-b:4,5-b′]dithiophene-2,6-diyl}{3-fluoro-2-[(2-ethylhexyl) carbonyl]thieno[3,4-b]thiophenediyl}) (PTB7) (Figure 1) —which when mixed with $PC_{71}BM$ was the first polymer solar cell to exhibit a power conversion efficiency over 7% (Ref. 91)—it has been reported by Yu and coworkers to have a coherence length of between only 3 and 4.5 π-π stacks (compared with 16 stacks for P3HT).[91] Salleo and coworkers have recently shown that high mobility can be maintained even in the case of low degree of order as determined by XRD. In these cases, local ordering (i.e., a few π-π stacks, not enough to give a strong signal in XRD), instead of long-range ordering, and extended backbones between these locally ordered aggregates allow for efficient transport through films.[75,92] In fact, long-range order is likely not even beneficial to charge-transport (when compared with short-range order) because the scattering mean free path of charge in π stacks is on the order of a nanometer.[75,93]

XRD is an appropriate tool to probe long-range order, but to probe the short-range ordering of a few molecular units in thin films UV-vis spectroscopy is more adept. Quantitative information about the local ordering of these films can be determined by fitting the weakly interacting H-aggregate model developed by Spano to UV-vis absorption spectra for P3ATs.[52,76,80,94,95] The absorption by a polymer thin film is the superposition of absorption by the ordered aggregates as well as the disordered amorphous regions of the film. The weakly interacting H-aggregate model calculates the absorption by the different vibronic states in the polymer aggregates—which when added together gives the total absorption by the aggregates—based on Gaussian fits to the experimental spectra using the following equation:

$$A(E) \propto \sum_{m=0}\left(\frac{S^m}{m!}\right) \times \left(1 - \frac{We^{-S}}{2E_p}\sum_{n\neq m}\frac{S^n}{n!(n-m)}\right)^2 \times \exp\left(\frac{-\left(E - E_{00} - mE_p - \frac{1}{2}WS^m e^{-S}\right)^2}{2\sigma^2}\right), \quad (5)$$

where *A* is the absorption by an aggregate as a function of the photon energy (*E*). *S* is the Huang-Rhys factor, which is calculated from absorption and emission spectra.[80] E_p is the intermolecular vibration energy and is determined by Raman spectroscopy. The variables *W*, σ, E_{00}, and a scaling factor are then adjusted to fit the model to the experimental spectrum. E_{00} is the energy of the $0 \rightarrow 0$ vibronic transition, which is allowed by assuming some disorder in the aggregates.[80] *W* is the free exciton bandwidth, which is related to the nearest neighbor interchain excitonic coupling. Upon coupling, a dispersion of the energies occurs, the width of which is equal to *W* (which is four times the nearest neighbor coupling). σ is the Gaussian linewidth and the terms *m* and *n* are the ground- and excited-state vibrational levels.

Once the absorption by the aggregates is calculated, it can then be subtracted from an experimental spectrum to determine the amount of absorption by the amorphous regions of the film. This information can then be used to estimate the proportion of aggregation in a sample. Additional information about the quality of the aggregates (e.g., *W*, which is inversely related to conjugation length) can also be determined from the weakly interacting H-aggregate model. This model has been used to look at the effects on electronic properties, mechanical properties, or both, of thin films due to solvent evaporation rates,[16] polymer side-chain length,[7] selection of different fullerene derivatives into the BHJs,[66] and cyclic straining of polymer films on elastomers (FOEs).[96]

III. DEFORMABILITY OF THIN-FILM ORGANIC SEMICONDUCTORS

The mechanical properties of bulk materials are rather straightforward to measure; however, the properties of thin-films can be considerably different due to skin-depth

effects.[97,98] Measuring the mechanical properties of thin-films by traditional bulk measurement techniques such as tensile testing is challenging because of the difficulty associated with isolating and manipulating a film of sub-micron thickness. To overcome these problems and measure the mechanical properties of thin films, several techniques have been developed. Many of these techniques rely on film-on-elastomer (FOE) systems, in which a thin film is either coated directly or transferred onto an elastomeric substrate. Properties such as the tensile modulus,[7,16,32,99] the strain at fracture (or crack-onset strain),[16,32,100] and the yield point,[98,101,102]—at least for FOE systems, which may be more relevant to real-world applications—can be readily measured by these techniques. The tensile modulus, E_{film}, is a measure of how a material accommodates strain in the elastic (or linear) regime of its stress-strain response. A low tensile modulus (highly deformable in the elastic regime) is prerequisite for applications requiring conformal bonding such as wearable[103–106] or implantable biosensors,[107,108] or more generally, any applications in which deformation occurs in two dimensions,[28] such as bonding to objects with geometries that are neither planar nor cylindrical.

The crack-onset strain (*CoS*), or the strain at which a film fractures on an elastomeric substrate, is a measure of ductility.[32,100] The *CoS* is, however, not an exact measurement of the failure point of a material—due to contributions from interlayer adhesion and the stress-strain response of the underlying substrate—but it is a qualitative measurement and has been well correlated to the tensile modulus of relatively low-molecular-weight conjugated polymers.[32] Measurement of *CoS* is necessary to inform design of devices expected to undergo strain, as selection of materials unable to accommodate the required strain will lead to film fracture and ultimately device failure. Similarly, the yield point—which is the strain at which a material begins to plastically or permanently deform—is important because as a film plastically deforms, its ordering changes; this change in microstructure is associated with changes in the electronic performance.[43,109] While plastic deformation can lead to chain alignment and improved mobility parallel to the axis of strain while the film is in the strained state, there is a disruption of aggregation and a decrease in mobility perpendicular to the strain.[43] A stress-strain curve for a hypothetical polymer is shown in Figure 7. Properties that can be easily measured by film-on-elastomer techniques (discussed below) are highlighted in green. Other properties important for mechanical robustness—but not measured by film-on-elastomer techniques—are the adhesion and cohesion of device layers.[68,110,111] While interlayer adhesion is important in deformable devices because poor adhesion will lead to delamination and high localized strain (and layer cracking), and similarly, cohesive fracture is a mode for intralayer failure, we will not focus on them in this review. (For readers interested in adhesion and cohesion, we direct them to the thorough work by Dauskardt and coworkers.)[31,67,110–115]

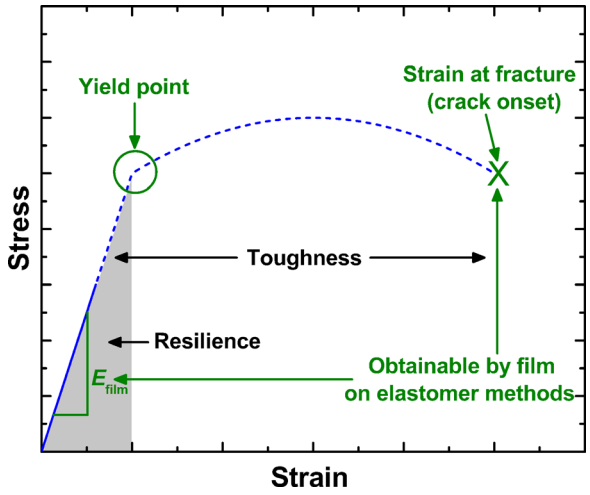

FIG. 7. The stress-strain response for a hypothetical polymer. The tensile modulus, E_{film}, the yield point, and the strain at fracture are obtainable by film on elastomer methods. Reproduced with permission from Printz *et al.*, ACS Appl. Mater. Interfaces **7**, 23257–23264 (2015). Copyright 2015 American Chemical Society.

A. Mechanical properties of films on elastomers

Stafford *et al.* developed a buckling-based metrology to measure the tensile modulus for FOE systems such as polystyrene and poly(methyl methacrylate).[97,99,116] In one incarnation of this technique, the material of interest is spun onto a glass slide and then transferred to an elastomeric substrate that has been strained a few percent before the film transfer. The strain is then released and the film then forms sinusoidal buckles out of plane (Figure 8(a)). The wavelength of the buckles is determined by the energy balance between the amount of energy it takes to deform the relatively soft elastomeric substrate and the amount of energy it takes to bend the relatively stiff thin film. The buckling wavelength has a linear dependence on the film thickness (e.g., thicker films are more rigid, which leads to an increase in the buckling wavelength). The tensile modulus of the film, E_{film}, can then be related to the buckling wavelength, λ_b, and the film thickness, d_f, as well as the tensile modulus of the elastomeric substrate, E_s, the Poisson's ratios of the thin film, ν_f, and the substrate, ν_s, by the following equation:[99]

$$E_{film} = 3E_s\left(\frac{1-\nu_f^2}{1-\nu_s^2}\right)\left(\frac{\lambda_b}{2\pi d_f}\right)^3. \quad (6)$$

This method has been used to determine the E_{film} of many polymers, including polystyrene and poly(methyl methacrylate),[97,99,117] poly(3-alkylthiophene)s,[7,16,32,57] and diketopyrrolopyrrole (DPP) based polymers.[30,118] Tahk and coworkers were the first to use this technique to measure the tensile modulus of conjugated polymers, including poly(3,4-ethylenedioxythiophene):poly(4-styrenesulfonate) (PEDOT:PSS), pentacene, P3HT, and a 1:0.8 blend of P3HT with [6,6]--phenyl C61-butyric acid methyl ester (PCBM).[119] The modulus of PEDOT:PSS was reported to be 2.26 ± 0.05 GPa (Figures 8(b) and 8(c)), while pentacene (16.09 ± 2.83 GPa), P3HT (1.33 ± 0.01 GPa), and P3HT:PCBM (6.02 ± 0.03 GPa) were also measured.[119] The much higher tensile modulus of pentacene when compared with the other materials tested was attributed to its polycrystallinity, while the polymeric systems were only semicrystalline. Another early buckling-based study on conjugated polymers explored the effect of

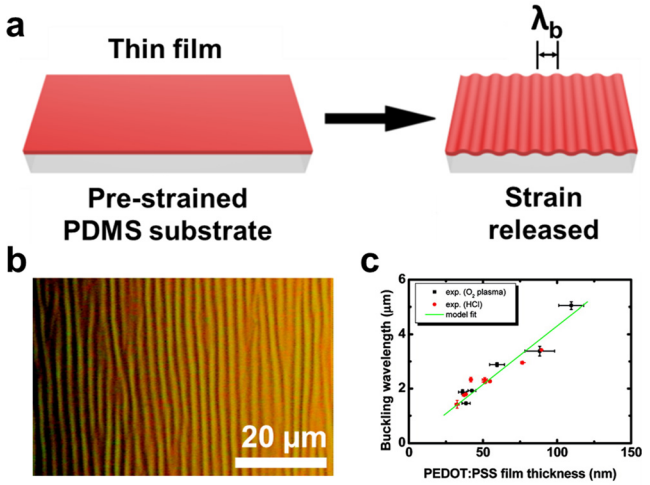

FIG. 8. Determination of the tensile modulus by the buckling-based metrology. (a) Schematic of one variation of the buckling procedure. A polymer thin film is transferred to a pre-strained polydimethylsiloxane (PDMS) substrate. The strain is released and the polymer buckles. The wavelength, λ_b, is related to the film stiffness and thickness. (b) Micrograph of a buckled film of PEDOT:PSS on PDMS. (c) Experimental data of buckling wavelength as a function of PEDOT:PSS film thickness. (b) and (c) Reproduced with permission from Tahk *et al.*, Macromolecules **42**, 7079–7083 (2009). Copyright 2009 American Chemical Society.

the modification of the polymer backbone on the tensile modulus,[30] The modulus of (poly(2,5-bis(2-octyldecyl)-3,6-di(thiophen-2-yl)diketopyrrolo[3,4-c]pyrrole-1,4-dione-alt-thieno[3,2-b]thiophene) (PDPPT-TT) (Figure 1), a polymer with a repeat unit of DPP flanked by two thiophene rings and thienothiophene, was compared with PDPPT-2T (Figure 1), which had a similar structure but replaced the thienothiophene unit with two thiophene rings.[30] The authors found that the PDPPT-TT had a higher modulus (0.99 GPa) than did PDPPT-2T (0.74 GPa) and attributed this observation to the fact that the stiffness of the fused rings of the thienothiophene unit in PDPPT-TT was greater than that of the isolated rings of the bithiophene unit in (poly(2,5-bis(2-octyldecyl)-3,6-di(thiophen-2-yl)diketopyrrolo[3,4-c]pyrrole-1,4-dione-alt-bithiophene) (PDPPT-2T).[15,30]

While the buckling method described above works well for materials with tensile moduli up to a few GPa, some materials are too stiff and crack upon transfer or upon the compression due to the prestrained elastomeric substrate being relaxed.[66,88,116] In this case, an intermediate layer can be used between the soft substrate and the more rigid film. It is important that the intermediate material has a known E_{film}, and it should be more deformable than the thin film of interest but less deformable than the substrate. From this stack, the effective tensile modulus, E_{eff}, can be calculated by the following equation:[66,116]

$$E_{eff} = \frac{1 + m^2 n^4 + 2mn(2n^2 + 3n + 2)}{(1+n)^3(1+mn)} E_{film,1} \quad \text{where}$$
$$m = \frac{E_{film,2}}{E_{film,1}}, \quad n = \frac{h_2}{h_1}, \tag{7}$$

where $E_{film,1}$ and $E_{film,2}$ are the moduli of the bottom and top films, respectively, and h_1 and h_2 are the thicknesses of the two films. The authors previously used this bilayer method to measure the E_{film} of fullerenes and found moduli between 5.1 and 25.6 GPa for technical grade $PC_{71}BM$ and 99% purity $PC_{61}BM$, respectively.[66,88]

In addition to the tensile modulus, other mechanical properties such as the strain at fracture (i.e., crack-onset) and the yield point can be measured by FOE methods. The *CoS* can be determined by observing the formation of cracks in a thin film on elastomer under increasing strain.[29,100] The yield point of a material, which is the strain at which it begins to plastically (i.e., permanently) deform, can be measured by two FOE techniques. The first involves the delamination of the film from the substrate and measurement of the curvature to determine the yield.[101] The FOE is compressed to force delamination before the strain is relaxed; the film is then annealed and at the point of delamination, a bump forms. The curvature of the bump and the thickness of the film are then used to calculate the yield point. Gurmessa and Croll used this method to determine the yield point of thin films of polystyrene and poly(2-vinylpyridine) (P2VP) homopolymers and block copolymers.[98,101] Another method to determine the yield point was recently proposed by our group by determining the onset of thin-film buckling using diffraction of light from a laser. This method—laser detection of yield point (LADYP)—subjects a polymer film on an elastic substrate to cycles of tensile strain that incrementally increase in steps of 1% (i.e., 0% → 1% → 0% → 2% → 0% → 3% → 0%, etc.), although any arbitrary increment can be used.[102] The formation of buckles manifests as a diffraction pattern obtained using a laser and represents the onset of plastic deformation, or the yield point of the polymer. With LADYP, a correlation between side-chain length and yield point was found in P3ATs, ranging from 5% strain for P3PT to 18% strain for P3OT.[102]

B. Other measurement techniques for mechanical properties of thin films

In addition to FOE methods, there are other techniques available to measure mechanical properties of thin films. The tensile modulus is commonly measured by nanoindentation, in which a film is indented with a tip mounted on a cantilever beam.[120,121] The load applied to the tip as well as its displacement into the film are measured; upon unloading the tip, the slope of the load-displacement line is correlated to E_{film}. However, the measurements produced by nanoindentation can be complicated by effects of the substrate and also the viscoelasticity of the polymer itself.[122] Another method to measure the mechanical properties of thin films, developed by Kim and coworkers, is similar to traditional bulk-sample tensile testing; a thin film is floated upon a liquid—water in the published studies—and a high resolution linear actuator strains the film while a highly sensitive load cell measures the stress.[59,123] A complete stress-strain curve can then be built from this information, however, but the method may be limited in certain instances due to the requirements that the liquid has high surface tension and low viscosity and that the thin film must be compatible with the liquid.[123] This method was used to measure the tensile

moduli of P3HT and copolymers of P3HT and P2VP and their blends with the fullerene derivative o-xylenyl C_{60} bis-adduct (OXCBA).[123] Complete stress-strain curves were later measured for P3HT films with varying regioregularity.[59] The authors found that as the regioregularity of the P3HT increased, the E_{film} increased as did the brittleness. These observations were attributed to the fact that polymer with higher regioregularity more readily formed aggregates, which are stiffer than the disorder polymer. Recently, Kim and coworkers used this same measurement technique to demonstrate that organic photovoltaics comprising an active layer blend of poly[4,8-bis(5-(2-ethylhexyl) thiophen-2-yl)benzo[1,2-b:4,5-b0]dithiophene-alt-1,3-bis(thiophen2-yl)-5-(2-hexyldecyl)-4H-thieno[3,4-c] pyrrole-4,6(5H)-dione] (PBDTTTPD) and poly[[N,N0-bis(2-hexyldecyl)-naphthalene-1,4,5,8-bis(dicarboximide)-2,6-diyl]-alt5,50-thiophene] (P(NDI2HD-T)) (Figure 1) exhibited a significant improvement in elongation at the point of fracture over blends of PBDTTTPD with PCBM (7.16% and 0.3%, respectively).[124]

IV. INHERENT COMPETITION BETWEEN DEFORMABILITY AND CHARGE TRANSPORT

In the limited literature where both the mechanical and electronic properties of conjugated polymers had been studied, an inherent competition between good electronic performance and high deformability or robustness had been observed.[15,16,59] O'Connor *et al*. reported that an increase in mobility was coupled with an increase in stiffness in the polythiophenes P3HT and PBTTT.[15] PBTTT was found to have higher mobility and stiffness than P3HT, which was attributed to differences in the side chain interactions. P3HT has side chains on every conjugated ring, while PBTTT has a thienothiophene spacer without sidechains. This spacer allows for intercalation of the sidechains which improves vertical registry and aggregation. Further ordering was observed when the PBTTT films were annealed at 180 °C, which coincided with an increase in both the mobility and tensile modulus (Figure 9(a)).[15,76,125] The solvent evaporation rate of films being deposited by solution has also been reported to affect the mechanical and electronic properties of organic semiconductors.[16] In blends of P3HT with the fullerene PCBM, Awartani *et al*. reported a correlation between photovoltaic *PCE* and modulus in spin coated films.[16] At a lower spin speed, the evaporation rate of the solvent is lower than at higher spin speeds; this lower evaporation rate results in improved film ordering as determined by the weakly interacting H-aggregate model.[16] The films spun at lower spin speeds (i.e., those with improved ordering) demonstrated a higher photovoltaic performance, but also higher stiffness, providing more evidence for an inherent competition between charge transport and deformability. Further support of this idea came from a study by Kim and coworkers which explored the effect of the regioregularity of P3HT on its properties.[59] They found that higher regioregularity led to higher mobility and tensile modulus—as well as higher brittleness—which was attributed to the improved order (Figure 9(b)).[59] The modulus ranged from 13 MPa for 64% regioregular P3HT to 287 MPa for 98% regioregularity, while the hole mobility ranged from 4.84×10^{-8} to 1.81×10^{-1} $cm^2\ V^{-1}\ s^{-1}$.[59]

In initial studies of another parameter known to effect the electronic and mechanical properties of polymers—the alkyl side-chain length—our group also found evidence supporting an inherent competition.[7,28,32] In P3ATs, we observed an increase in deformability and ductility with increasing side-chain length. Interestingly, an order of magnitude decrease in E_{film} was found between P3HT, $n = 6$, and P3OT, $n = 8$ from 1.09 ± 0.15 GPa to 0.15 ± 0.05 GPa.[32] A large increase in the crack-onset strain was also observed between P3HT and P3OT (Figure 10(a)).[32] To better understand the practical implications of the observed reduction in modulus and increase in crack-onset strain, thin films

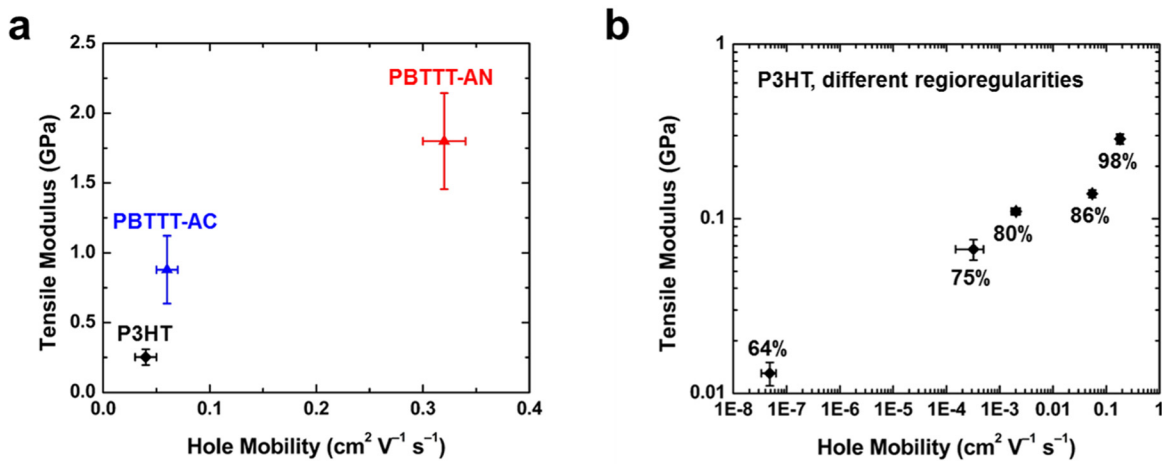

FIG. 9. Tensile modulus vs. hole mobility for polythiophenes. (a) The tensile modulus and hole mobility of P3HT are lower than that of PBTTT. Both the stiffness and hole mobility increase when as cast PBTTT (PBTTT-AC) is annealed at 180 °C (PBTTT-AN). The increase in tensile modulus and mobility of PBTTT compared with P3HT is attributed to improved order in PBTTT. Further ordering occurs in PBTTT when it is annealed, also leading to improved mobility and increased stiffness. (b) The tensile modulus and hole mobility of P3HT simultaneously increase with increasing regioregularity of the side-chains. The increase in both properties is likely due to the increased ability of regioregular P3HT to form ordered aggregates, which have improved charge transport properties, but is also stiff. (a) Reproduced with permission from O'Connor *et al*., ACS Nano **4**, 7538–7544 (2010). Copyright 2010 American Chemical Society.

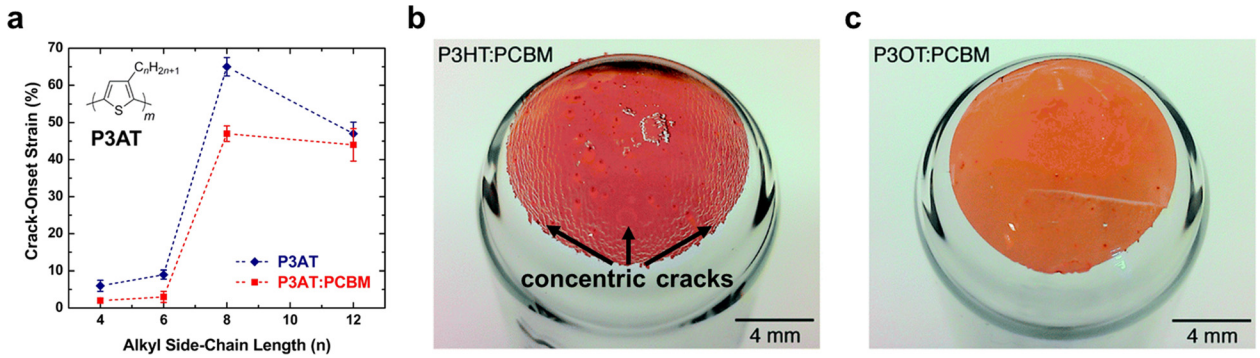

FIG. 10. Ductility of P3ATs and its blends with PCBM. (a) The crack-onset strain of P3ATs and P3AT:PCBM blends as a function of side-chain length. The largest observed increase was between P3HT and P3OT. (b) When the relatively stiff P3HT was blended 1:1 with PCBM and transferred to a hemisphere requiring 24% strain accommodation, the film cracked radially. (c) 1:1 P3OT:PCBM did not crack when transferred because of its higher deformability. (b) and (c) Reproduced with permission from O'Connor *et al*., Energy Environ. Sci. **7**, 370–378 (2014). Copyright 2014 The Royal Society of Chemistry.

comprising 1:1 blends of P3HT and P3OT with fullerenes were then stretched over glass hemispheres.[28] Finite element analysis calculated that these films would be required to accommodate 24% strain. While devices with the P3OT:PCBM active layer accommodated the strain without fracturing, devices with the P3HT:PCBM active layer fractured radially resulting in shorting (Figures 10(b) and 10(c)). However, even though P3OT:PCBM could accommodate the strain, its *PCE* was very low ($\eta = 0.36\%$).[28]

V. IMPROVING DEFORMABILITY WITHOUT SACRIFICING ELECTRONIC PERFORMANCE

Ideally, organic semiconductors would demonstrate both high electronic performance and mechanical robustness (e.g., a low tensile modulus and high crack-onset, yield point, resilience, and toughness). To date, a few strategies have been uncovered as potential pathways for achieving co-optimization of electronic performance and intrinsic deformability. Almost all of these strategies employ a delicate balance of stiffer, semiconducting (or conducting) polymer with softer, insulating material—enough to improve deformability, but not too much as to destroy charge transport. For example, as discussed above, papers by Savagatrup *et al*. and O'Connor *et al*. found that as the side-chain length increased in P3ATs, the tensile modulus decreased, but so too did the power conversion efficiency.[7,32] The largest decrease in tensile modulus was observed between P3HT, $n = 6$, and P3OT, $n = 8$, which corresponded with a significant decrease in *PCE*. We thus sought to combine the properties of P3HT with those of P3OT in an effort to co-optimize electronic performance and deformability by exploring P3ATs with an average side-chain length, $n = 7$. We synthesized 1:1 block and random co-polymers of P3HT and P3OT and also explored the properties of a physical blend of P3HT and P3OT, as well as the homopolymers poly(3-heptylthiophene) (P3HpT, $n = 7$) (Figure 11(a)).[7] Figure 11(b) is a graph of the *PCE* against the tensile moduli of these polymers. If you imagine a line connecting the P3HT and P3OT points in Figure 11(b), materials with more favorable properties would lie above and to the left of this line, which essentially just the average of the homopolymer properties. The properties of the block copolymer, P3HT-*b*-

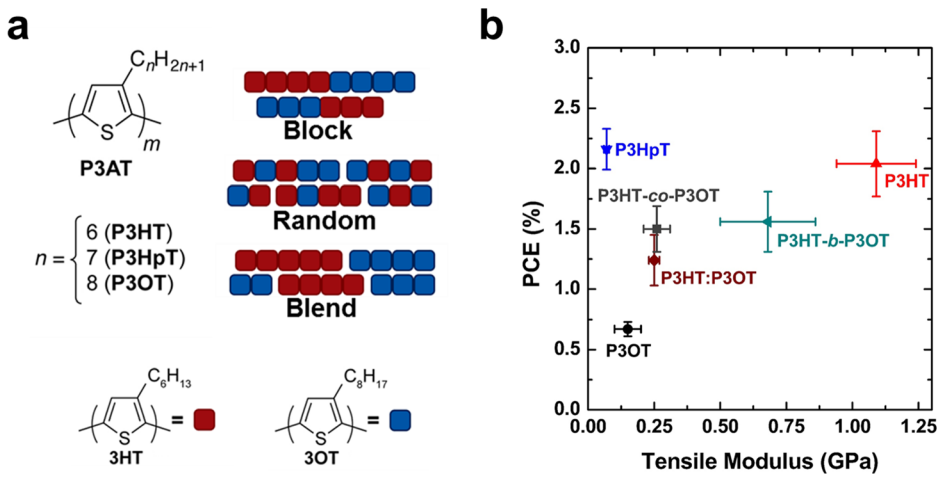

FIG. 11. Finding co-optimization of electronic properties and deformability in P3ATs. (a) P3ATs with an average side-chain length of $n = 7$ were tested, including a block and random copolymer of P3HT ($n = 6$) and P3OT ($n = 8$), a physical blend of the two homopolymers, and a P3HpT ($n = 7$). (b) OPV power conversion efficiency (*PCE*) versus the tensile modulus of the P3ATs. OPV devices were fabricated with a PEDOT:PSS bottom electrode, an active layer comprising a 1:1 polymer:$PC_{61}BM$ blend, and a eutectic Gallium-Indium (eGaIn) liquid metal as the top electrode. Reproduced with permission from Savagatrup *et al*., Macromolecules **47**, 1981–1992 (2014). Copyright 2014 American Chemical Society.

P3OT, are seemingly an average of the two homopolymers. The random copolymer, P3HT-*co*-P3OT, and the homopolymers blend, P3HT:P3OT, exhibit a slightly more favorable combination of properties than the block copolymer as they lie just above the average. P3HpT, however, lies well above the average of the homopolymers and has the favorable deformability of P3OT and photovoltaic performance of P3HT.[7] Interestingly, the μ_h of P3HpT is 0.0005 $cm^2\ V^{-1}\ s^{-1}$, over an order of magnitude lower than that of P3HT (0.011 $cm^2\ V^{-1}\ s^{-1}$), and of the same order of magnitude as P3OT (0.0001 $cm^2\ V^{-1}\ s^{-1}$).[57] However, upon blending in a 1:1 ratio with PCBM, the μ_h of P3HpT increases to 0.004 $cm^2\ V^{-1}\ s^{-1}$, which is on the same order of magnitude as the blend of P3HT:PCBM (0.010 $cm^2\ V^{-1}\ s^{-1}$).[57] This increase in mobility upon addition of PCBM is likely why P3HpT performs similarly in photovoltaic devices as P3HT. Additionally, we attributed that the low tensile modulus to the T_g of P3HpT, which at −5 °C (as measured by differential scanning calorimetry), is similar to P3OT (−10 °C) and much lower than P3HT (12 °C), which is close to room temperature.[57]

While increasing the deformability of conjugated polymers by including the soft, insulating material as side-chains—away from the polymer backbone where they will not affect electronic properties—is a successful strategy for co-optimization, another demonstrated strategy has been to covalently bind blocks of softer material directly into the backbone of the polymer. Müller and coworkers found that diblock copolymers of P3HT and the insulating polyethylene (PE)—which both form well-ordered domains—demonstrated not only improved mechanical properties but also improved μ_h of OFETs.[5] Transistors with the semiconductor comprising diblock copolymers of 35:65 (Figure 12(a)) and 10:90 P3HT:PE exhibited mobilities of 0.05 and 0.02 $cm^2\ V^{-1}\ s^{-1}$, respectively, while transistors with P3HT homopolymer only had a mobility of 0.01 $cm^2\ V^{-1}\ s^{-1}$.[5] In addition to this improvement in mobility, the ductility of the diblock copolymers was also significantly higher; the *CoS* increased from 13% for the pure P3HT to over 600% for both of the diblock copolymers (Figure 12(b)).[5] It should be noted that while films of the diblock copolymers were significantly more ductile than those of the P3HT homopolymer, they were also much stiffer. Interestingly, the tensile modulus of the diblock copolymers (240 MPa for the 35:65 copolymer) was about an order of magnitude higher than that of the P3HT homopolymer (28 MPa).[5] Kim and coworkers found that adding 5% block and graft (a slight variation to the backbone linking, but resulting in similar behavior) copolymers of P3HT and P2VP to P3HT (and P3HT:fullerene) films actually resulted in a reduction of tensile modulus (and improved cohesive fracture energy) when compared with P3HT homopolymer films, without deleterious effects on the performance in polymer:fullerene OPV devices (Figures 12(c)–12(e)).[123] Recently, Qiu and coworkers made ABA triblock copolymer of P3HT (A) and poly(methyl acrylate) (B) and reported that the material had a tensile modulus of only 6 MPa, an elongation at break of 140%, and a mobility of 9×10^{-4} $cm^2\ V^{-1}\ s^{-1}$ (compared with 4.5×10^{-4} $cm^2\ V^{-1}\ s^{-1}$ for P3HT homopolymer).[126] Although the authors did not report any measurements of the mechanical

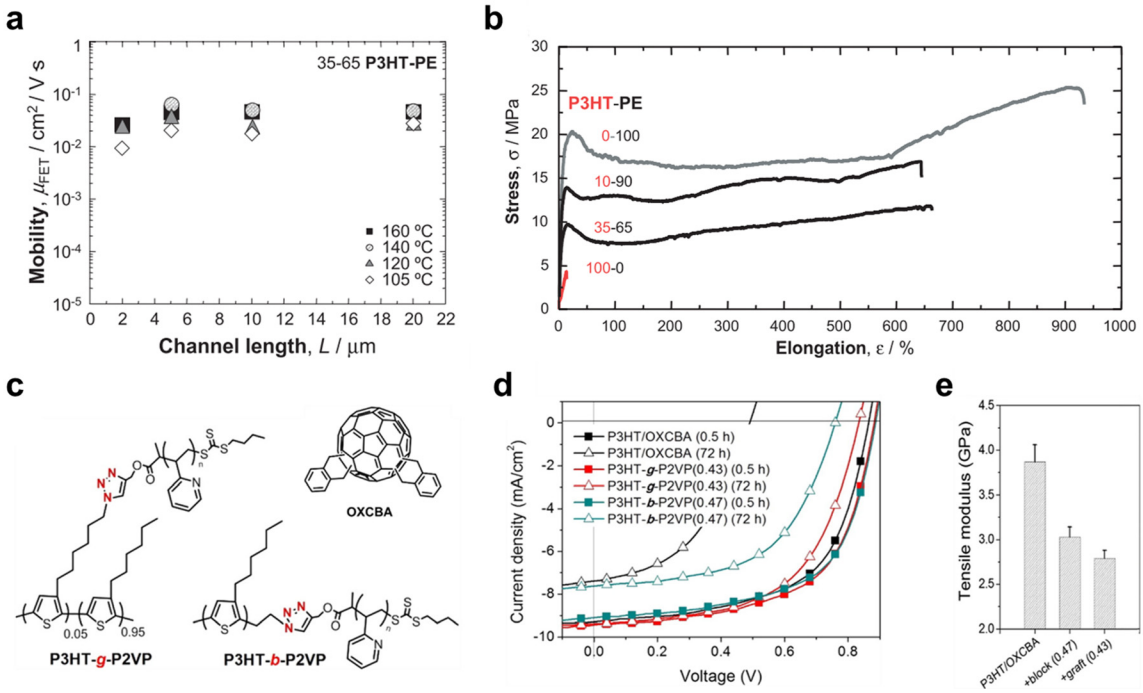

FIG. 12. Copolymerization of P3HT and its effects on electronic and mechanical properties. (a) The hole mobility in a 35:65 block copolymer of P3HT and PE as a function of OFET channel length. (b) Stress-strain responses of bulk P3HT-*b*-PE copolymers. (c) The molecular structures of the graft copolymer, P3HT-*g*-P2VP, and the block copolymer, P3HT-*b*-P2VP, and the fullerene o-xylenyl C_{60} bis-adduct (OXCBA). (d) *J-V* curves of devices made with BHJs of P3HT:OXCBA as well as with 5% copolymer added. The numbers in parenthesis following P2VP are the volume fraction of P3HT in the P3HT-*g*-P2VP and P3HT-*b*-P2VP. (e) The decreasing tensile modulus of polymer:OXCBA blends with the addition of the copolymers of P3HT and P2VP. (a) and (b) Reproduced with permission from Müller *et al.*, Adv. Funct. Mater. **17**, 2674–2679 (2007). Copyright 2007 Wiley-VCH Verlag GmbH & Co. KGaA. (c)–(e) Reproduced with permission from Kim *et al.*, ACS Nano **8**, 10461–10470 (2014). Copyright 2014 American Chemical Society.

properties of P3HT homopolymer, the tensile modulus and elongation at break were below the P3HT-*b*-PE values reported by Müller and coworkers.[5]

P3ATs and their copolymers are terrific model systems due to their simplicity, but low-bandgap polymers, comprising donor and acceptor units covalently bound, have become a primary focus in the field because they absorb more of the solar spectrum than do homopolymers. While performance is improved in these low-bandgap polymers compared with homopolymers, they incorporate fused aromatic rings along the polymer backbone, making them relatively stiffer than polymers with unfused rings along the backbone.[30] Since the primary goal in the field of organic electronics research has been to improve electronic properties, the increase in stiffness is often ignored in pursuit of performance. As we have argued throughout this review, though, researchers should keep in mind that the likely applications for completed devices will require deformability. There has not been much work in improving the mechanical properties of low-bandgap polymers, but our group previously published a study that demonstrated a decreased stiffness in a DPP-based polymer.[118] We hypothesized that slightly disrupting the ordering of these polymers would lead to more deformable materials. DPP units were selected as the basis for the polymer backbone because they are common in literature due to the ease of their synthesis. To that end, we introduced random segments of unlike monomer—a terthiophene with two rings with alkyl side-chain substituents and a third unsubstituted thiophene ring—into the polymer PDPP2FT, which consisted of a DPP unit flanked by two furans and a thiophene.[118] The addition of these random segments decreased the E_{film} from 2.17 GPa for the pure PDPP2FT to 0.93 GPa without having a deleterious effect on the *PCE*.[118] The dearth of literature on improvement of the mechanical properties of high-performance low-bandgap polymers is not, in our opinion, indicative of an impossible task. Rather, we believe that it is due to a lack of research efforts so far and that this area is likely to be fruitful for those who decide to take on the challenge.

Another strategy for potentially co-optimizing properties that we believe warrants that further exploration is the addition of plasticizing additives into semiconducting layers. Additives such as 1,8-diiodooctane (DIO) and low molecular weight polydimethylsiloxane (PDMS) have been shown to improve OPV performance.[127,128] While there were no individual studies on both the mechanical and electronic properties of the same material with the inclusion of additives, separate studies on electronic and mechanical properties suggest additives as a viable pathway to co-optimization of properties. Lee *et al.* showed that the addition of DIO to blends of [2,6-(4,4-bis(2-ethylhexyl)-4H-cyclopenta[2,1b;3,4-b′]-dithiophene)-alt-4,7-(2,1,3-benzothiadiazole)] (PCPDTBT) (Figure 1) with $PC_{71}BM$ improved the photovoltaic device efficiency from 3.35% to 5.12%.[127] Reynolds and coworkers showed that the addition of small concentrations of low molecular weight PDMS ($\sim$0.1 mg ml^{-1}) to a thiophene and isoindigo-based small molecule improved the photovoltaic efficiency of its blend with $PC_{61}BM$ from 1.25% to 2.16%.[128] These additives were also found to decrease the tensile modulus of blends of P3HT:$PC_{61}BM$, from 1.23 GPa for the additive-free blend to 0.88 GPa with the PDMS additive and 0.38 with the DIO additive.[32] The decrease in tensile modulus observed by the authors was attributed to the plasticizing effects, or increasing free volume, but could also be due to changes in the morphology of the films. Additives are a promising route to co-optimization, but it should be noted that the effects of additives across various conjugated polymers may be unequal. These differences require additional parameters to be optimized for each system—e.g., finding the appropriate additive and its concentration.

There is one commonly implemented strategy to create stretchable devices exhibiting stable electronic performance under strain that does not require intrinsically deformable organic semiconductors. This strategy, which has been demonstrated several times for OPV devices, utilizes an elastomeric substrate which is pre-strained (usually to the strain the device is expected to undergo) and then coated with an active material/device before the strain is subsequently released.[6,104,129] The procedure is essentially identical to the buckling procedure used to measure the tensile modulus of thin films—except the pre-strain is usually greater—and the result is the same; the stiffer film atop the elastomeric substrate will buckle out of plane and accommodate at least as much strain at the elastomer was pre-strained. However, the roughened surface due to the buckling can be undesirable in many applications (e.g., displays), and the requirement of having to pre-strain the elastomeric substrate makes this strategy less amenable to roll-to-roll processing than simply using conjugated polymers that exhibit intrinsic deformability.

VI. CONCLUSION AND FUTURE DIRECTIONS

A key advantage of organic semiconductors is the potential for intrinsic deformability and robustness, allowing them to be ideal candidates for integration into wearable, implantable, and roll-to-roll printable devices. The integration of organic semiconductors into devices that will undergo bending, stretching, conformal bonding, or some combination thereof requires anticipation of not only the electronic performance of these materials but also their mechanical performance. We stress that researchers should not assume mechanical robustness and deformability of organic semiconductors and instead verify these properties when developing new materials. To bridge these areas of research, we provided a high-level introduction to some of the important electronic and mechanical properties and measurement techniques for organic electronic devices. We also explored the inherent competition between good electronic performance and mechanical robustness (and specifically deformability) and highlighted several strategies for overcoming this undesirable competition. Pathways to co-optimization include incorporating softer, insulating materials into a stiffer, semiconducting (or conducting) polymer, and promotion of disorder in aggregation. However, there is a delicate balance and care must be taken to ensure that increased deformability does not come at the expense of electronic properties. One can think of this challenge as "living on the edge"—pushing

the mechanical deformability as far as it can go before electronic performance falls off the edge of a cliff.

Co-optimization of electronic performance and deformability and robustness is likely to continue to be a rich area of research for the foreseeable future. For instance, although pathways to co-optimization have been identified, it is still unknown whether or not these effects apply universally to organic semiconductors, or to just a few specific families. With countless new semiconducting polymers and polymer families being invented every year, it would be a herculean task for only one or a few groups to catalog the mechanical properties of all of these materials. Instead, the onus is on all researchers in the field to understand the mechanical properties of the materials they are producing (and ideally design new materials with mechanical properties in mind). Obviously, this argument works in the other direction as well; the mechanical properties of the current highest performing polymer semiconductors must also be understood. Further work also needs to be performed in the identification of additional design rules for co-optimization, especially in OPV as researchers move away from the use of fullerene electron acceptors and toward new polymers and small molecules, which will likely have different intermolecular interactions with common electron donors. While computational modeling has previously been implemented to give a molecular explanation to the observed mechanical properties of previously fabricated systems,[51,113] it would be ideal to develop a predictive model for properties of new or not yet synthesized organic semiconductors.[130] This predictive modeling would allow scientists and engineers to easily design or select the best material for specific applications. Ultimately, the goal of this review is to stimulate further research in an area of increasing importance as research in organic semiconductors matures to device design and implementation.

ACKNOWLEDGMENTS

This work was supported by the Air Force Office of Scientific Research (AFOSR) Young Investigator Program, Grant No. FA9550-13-1-0156 and laboratory startup funds from the University of California, San Diego.

[1]Y. Yuan, G. Giri, A. L. Ayzner, A. P. Zoombelt, S. C. B. Mannsfeld, J. Chen, D. Nordlund, M. F. Toney, J. Huang, and Z. Bao, "Ultra-high mobility transparent organic thin film transistors grown by an off-centre spin-coating method," Nat. Commun. **5**, 3005 (2014).
[2]Z. He, C. Zhong, S. Su, M. Xu, H. Wu, and Y. Cao, "Enhanced power-conversion efficiency in polymer solar cells using an inverted device structure," Nat. Photonics **6**, 593–597 (2012).
[3]L. Dou, J. You, Z. Hong, Z. Xu, G. Li, R. A. Street, and Y. Yang, "25Th anniversary article: A decade of organic/polymeric photovoltaic research," Adv. Mater. **25**, 6642–6671 (2013).
[4]M. Riede, C. Uhrich, J. Widmer, R. Timmreck, D. Wynands, G. Schwartz, W. M. Gnehr, D. Hildebrandt, A. Weiss, J. Hwang *et al.*, "Efficient organic tandem solar cells based on small molecules," Adv. Funct. Mater. **21**, 3019–3028 (2011).
[5]C. Müller, S. Goffri, D. W. Breiby, J. W. Andreasen, H. D. Chanzy, R. A. J. Janssen, M. M. Nielsen, C. P. Radano, H. Sirringhaus, P. Smith *et al.*, "Tough, semiconducting polyethylene-poly(3-Hexylthiophene) diblock copolymers," Adv. Funct. Mater. **17**, 2674–2679 (2007).
[6]M. Kaltenbrunner, M. S. White, E. D. Głowacki, T. Sekitani, T. Someya, N. S. Sariciftci, and S. Bauer, "Ultrathin and lightweight organic solar cells with high flexibility," Nat. Commun. **3**, 770 (2012).
[7]S. Savagatrup, A. D. Printz, D. Rodriquez, and D. J. Lipomi, "Best of both worlds: Conjugated polymers exhibiting good photovoltaic behavior and high tensile elasticity," Macromolecules **47**, 1981–1992 (2014).
[8]S. Savagatrup, A. D. Printz, T. F. O'Connor, A. V. Zaretski, and D. J. Lipomi, "Molecularly stretchable electronics," Chem. Mater. **26**, 3028–3041 (2014).
[9]T. Li, Z. Suo, S. P. Lacour, and S. Wagner, "Compliant thin film patterns of stiff materials as platforms for stretchable electronics," J. Mater. Res. **20**, 3274–3277 (2005).
[10]D. H. Kim, N. S. Lu, R. Ma, Y. S. Kim, R. H. Kim, S. D. Wang, J. Wu, S. M. Won, H. Tao, A. Islam *et al.*, "Epidermal electronics," Science (80-) **333**, 838–844 (2011).
[11]A. Polywka, T. Jakob, L. Stegers, T. Riedl, and P. Görrn, "Facile preparation of high-performance elastically stretchable interconnects," Adv. Mater. **27**, 3755–3759 (2015).
[12]Z. Yu, X. Niu, Z. Liu, and Q. Pei, "Intrinsically stretchable polymer light-emitting devices using carbon nanotube-polymer composite electrodes," Adv. Mater. **23**, 3989–3994 (2011).
[13]J. Mei and Z. Bao, "Side chain engineering in solution-processable conjugated polymers," Chem. Mater. **26**, 604–615 (2014).
[14]P. Boufflet, Y. Han, Z. Fei, N. D. Treat, R. Li, D.-M. Smilgies, N. Stingelin, T. D. Anthopoulos, and M. Heeney, "Using molecular design to increase hole transport: Backbone fluorination in the benchmark material poly(2,5-bis(3-alkylthiophen-2-yl)thieno[3,2-*b*]-thiophene (pBTTT)," Adv. Funct. Mater. **25**, 7038–7048 (2015).
[15]B. O'Connor, E. P. Chan, C. Chan, B. R. Conrad, L. J. Richter, R. J. Kline, M. Heeney, I. McCulloch, C. L. Soles, and D. M. DeLongchamp, "Correlations between mechanical and electrical properties of polythiophenes," ACS Nano **4**, 7538–7544 (2010).
[16]O. Awartani, B. I. Lemanski, H. W. Ro, L. J. Richter, D. M. DeLongchamp, and B. T. O'Connor, "Correlating stiffness, ductility, and morphology of polymer:fullerene films for solar cell applications," Adv. Energy Mater. **3**, 399–406 (2013).
[17]M. Shin, J. H. Song, G. H. Lim, B. Lim, J. J. Park, and U. Jeong, "Highly stretchable polymer transistors consisting entirely of stretchable device components," Adv. Mater. **26**, 3706–3711 (2014).
[18]R. Po, C. Carbonera, A. Bernardi, F. Tinti, and N. Camaioni, "Polymer- and carbon-based electrodes for polymer solar cells: Toward low-cost, continuous fabrication over large area," Sol. Energy Mater. Sol. Cells **100**, 97–114 (2012).
[19]N. Espinosa, M. Hösel, D. Angmo, and F. C. Krebs, "Solar cells with one-day energy payback for the factories of the future," Energy Environ. Sci. **5**, 5117–5132 (2012).
[20]A. Anctil, C. W. Babbitt, R. P. Raffaelle, and B. J. Landi, "Cumulative energy demand for small molecule and polymer photovoltaics," Prog. Photovoltaics **21**, 1541–1554 (2013).
[21]F. C. Krebs, "Fabrication and processing of polymer solar cells: A review of printing and coating techniques," Sol. Energy Mater. Sol. Cells **93**, 394–412 (2009).
[22]R. R. Søndergaard, M. Hösel, and F. C. Krebs, "Roll-to-roll fabrication of large area functional organic materials," J. Polym. Sci., Part B: Polym. Phys. **51**, 16–34 (2013).
[23]H. A. Becerril, J. Mao, Z. Liu, R. M. Stoltenberg, Z. Bao, and Y. Chen, "Evaluation of solution-processed reduced graphene oxide films as transparent conductors," ACS Nano **2**, 463–470 (2008).
[24]Y. Diao, Y. Zhou, T. Kurosawa, L. Shaw, C. Wang, S. Park, Y. Guo, J. A. Reinspach, K. Gu, X. Gu *et al.*, "Flow-enhanced solution printing of all-polymer solar cells," Nat. Commun. **6**, 7955 (2015).
[25]A. De La Fuente Vornbrock, D. Sung, H. Kang, R. Kitsomboonloha, and V. Subramanian, "Fully gravure and ink-jet printed high speed pBTTT organic thin film transistors," Org. Electron. **11**, 2037–2044 (2010).
[26]F. C. Krebs, M. Biancardo, B. Winther-Jensen, H. Spanggard, and J. Alstrup, "Strategies for incorporation of polymer photovoltaics into garments and textiles," Sol. Energy Mater. Sol. Cells **90**, 1058–1067 (2006).
[27]G. Schwartz, B. C.-K. Tee, J. Mei, A. L. Appleton, D. H. Kim, H. Wang, and Z. Bao, "Flexible polymer transistors with high pressure sensitivity for application in electronic skin and health monitoring," Nat. Commun. **4**, 1859 (2013).
[28]T. F. O'Connor, A. V. Zaretski, B. A. Shiravi, S. Savagatrup, A. D. Printz, M. I. Diaz, and D. J. Lipomi, "Stretching and conformal bonding of organic solar cells to hemispherical surfaces," Energy Environ. Sci. **7**, 370–378 (2014).
[29]S. Savagatrup, A. D. Printz, T. F. O'Connor, A. V. Zaretski, D. Rodriquez, E. J. Sawyer, K. M. Rajan, R. I. Acosta, S. E. Root, and D. J.

Lipomi, "Mechanical degradation and stability of organic solar cells: Molecular and microstructural determinants," Energy Environ. Sci. **8**, 55–80 (2015).
[30]D. J. Lipomi, H. Chong, M. Vosgueritchian, J. Mei, and Z. Bao, "Toward mechanically robust and intrinsically stretchable organic solar cells: Evolution of photovoltaic properties with tensile strain," Sol. Energy Mater. Sol. Cells **107**, 355–365 (2012).
[31]C. Bruner, N. C. Miller, M. D. McGehee, and R. H. Dauskardt, "Molecular intercalation and cohesion of organic bulk heterojunction photovoltaic devices," Adv. Funct. Mater. **23**, 2863–2871 (2013).
[32]S. Savagatrup, A. S. Makaram, D. J. Burke, and D. J. Lipomi, "Mechanical properties of conjugated polymers and polymer-fullerene composites as a function of molecular structure," Adv. Funct. Mater. **24**, 1169–1181 (2014).
[33]M. T. Sajjad, A. J. Ward, C. Kästner, A. Ruseckas, I. D. W. Samuel, H. Hoppe, and I. D. W. Samuel, "Controlling exciton diffusion and fullerene distribution in photovoltaic blends by side chain modification," J. Phys. Chem. Lett. **6**, 3054–3060 (2015).
[34]S. Himmelberger, D. T. Duong, J. E. Northrup, J. Rivnay, F. P. V. Koch, B. S. Beckingham, N. Stingelin, R. A. Segalman, S. C. B. Mannsfeld, and A. Salleo, "A. role of side-chain branching on thin-film structure and electronic properties of polythiophenes," Adv. Funct. Mater. **25**, 2616–2624 (2015).
[35]G. Li, Y. Yao, H. Yang, V. Shrotriya, G. Yang, and Y. Yang, ""Solvent annealing" effect in polymer solar cells based on poly(3-Hexylthiophene) and methanofullerenes," Adv. Funct. Mater. **17**, 1636–644 (2007).
[36]L. H. Nguyen, H. Hoppe, T. Erb, S. Günes, G. Gobsch, and N. S. Sariciftci, "Effects of annealing on the nanomorphology and performance of poly(alkylthiophene):fullerene bulk-heterojunction solar cells," Adv. Funct. Mater. **17**, 1071–1078 (2007).
[37]E. Verploegen, R. Mondal, C. J. Bettinger, S. Sok, M. F. Toney, and Z. Bao, "Effects of thermal annealing upon the morphology of polymer-fullerene blends," Adv. Funct. Mater. **20**, 3519–3529 (2010).
[38]S. Salammal, E. Mikayelyan, S. Grigorian, U. Pietsch, N. Koenen, U. Scherf, M. Brinkmann, and N. Kayunkid, "Impact of thermal annealing on the semicrystalline nanomorphology of spin-coated thin films of regioregular poly (3-alkylthiophene) S as observed by high-resolution transmission electron microscopy and grazing incidence X-ray diffraction," Macromolecules **45**, 5575–5585 (2012).
[39]W. Huang, E. Gann, Y.-B. Cheng, and C. R. McNeill, "In-depth understanding of the morphology–performance relationship in polymer solar cells," ACS Appl. Mater. Interfaces **7**, 14026–14034 (2015).
[40]M. Brinkmann and J.-C. Wittmann, "Orientation of regioregular poly(3-hexylthiophene) by directional solidification: A simple method to reveal the semicrystalline structure of a conjugated polymer," Adv. Mater. **18**, 860–863 (2006).
[41]X. Zhang, L. J. Richter, D. M. Delongchamp, R. J. Kline, M. R. Hammond, I. McCulloch, M. Heeney, R. S. Ashraf, J. N. Smith, T. D. Anthopoulos *et al.*, "Molecular packing of high-mobility diketo pyrrolo-pyrrole polymer semiconductors with branched alkyl side chains," J. Am. Chem. Soc. **133**, 15073–15084 (2011).
[42]J. Liu, Y. Sun, X. Gao, R. Xing, L. Zheng, S. Wu, Y. Geng, and Y. Han, "Oriented poly(3-hexylthiophene) nanofibril with the π-π stacking growth direction by solvent directional evaporation," Langmuir **27**, 4212–4219 (2011).
[43]B. O'Connor, R. J. Kline, B. R. Conrad, L. J. Richter, D. Gundlach, M. F. Toney, and D. M. DeLongchamp, "Anisotropic structure and charge transport in highly strain-aligned regioregular poly(3-hexylthiophene)," Adv. Funct. Mater. **21**, 3697–3705 (2011).
[44]D. Gargi, R. J. Kline, D. M. DeLongchamp, D. A. Fischer, M. F. Toney, and B. T. O'Connor, "Charge transport in highly face-on poly(3-hexylthiophene) films," J. Phys. Chem. C **117**, 17421–17428 (2013).
[45]B. Kitchen, O. Awartani, R. J. Kline, T. McAfee, H. Ade, and B. T. O'Connor, "Tuning open-circuit voltage in organic solar cells with molecular orientation," ACS Appl. Mater. Interfaces **7**, 13208–13216 (2015).
[46]S. Himmelberger, K. Vandewal, Z. Fei, M. Heeney, and A. Salleo, "Role of molecular weight distribution on charge transport in semiconducting polymers," Macromolecules **47**, 7151–7157 (2014).
[47]R. J. Kline, M. D. McGehee, E. N. Kadnikova, J. Liu, and J. M. J. Fréchet, "Controlling the field-effect mobility of regioregular polythiophene by changing the molecular weight," Adv. Mater. **15**, 1519–1522 (2003).
[48]A. Zen, M. Saphiannikova, and D. Neher, "Effect of molecular weight on the structure and crystallinity of poly (3-hexylthiophene)," Macromolecules **39**, 2162–2171 (2006).
[49]R. Zhang, B. Li, M. C. Iovu, M. Jeffries-el, G. Sauve, J. Cooper, S. Jia, S. Tristram-Nagle, D. M. Smilgies, D. N. Lambeth *et al.*, "Nanostructure dependence of field-effect mobility in regioregular poly (3-hexylthiophene) thin film field effect transistors nanostructure dependence of field-effect mobility in regioregular," J. Am. Chem. Soc. **128**, 3480–3481 (2006).
[50]K. Zhao, H. U. Khan, R. Li, Y. Su, and A. Amassian, "Entanglement of conjugated polymer chains influences molecular self-assembly and carrier transport," Adv. Funct. Mater. **23**, 6024–6035 (2013).
[51]N. R. Tummala, C. Risko, C. Bruner, R. H. Dauskardt, and J.-L. Brédas, "Entanglements in P3HT and their influence on thin-film mechanical properties: Insights from molecular dynamics simulations," J. Polym. Sci., Part B: Polym. Phys. **53**, 934–942 (2015).
[52]J. Clark, J.-F. Chang, F. C. Spano, R. H. Friend, and C. Silva, "Determining exciton bandwidth and film microstructure in polythiophene films using linear absorption spectroscopy," Appl. Phys. Lett. **94**, 163306 (2009).
[53]J. Chang, B. Sun, D. W. Breiby, M. M. Nielsen, T. I. Solling, M. Giles, I. McCulloch, and H. Sirringhaus, "Enhanced mobility of poly (3-hexylthiophene) transistors by spin-coating from high-boiling-point solvents," Chem. Mater. **16**, 4772–4776 (2004).
[54]H. Jia, S. Gowrisanker, G. K. Pant, R. M. Wallace, and B. E. Gnade, "Effect of poly (3-hexylthiophene) film thickness on organic thin film transistor properties," J. Vac. Sci. Technol., A **24**, 1228–1232 (2006).
[55]L. A. Majewski, J. W. Kingsley, C. Balocco, and A. M. Song, "Influence of processing conditions on the stability of poly(3-hexylthiophene)-based field-effect transistors," Appl. Phys. Lett. **88**, 222108 (2006).
[56]M. Surin, P. Leclére, R. Lazzaroni, J. D. Yuen, G. Wang, D. Moses, A. J. Heeger, S. Cho, and K. Lee, "Relationship between the microscopic morphology and the charge transport properties in poly(S-hexylthiophene) field-effect transistors," J. Appl. Phys. **100**, 033712 (2006).
[57]S. Savagatrup, A. D. Printz, H. Wu, K. M. Rajan, E. J. Sawyer, A. V. Zaretski, C. J. Bettinger, and D. J. Lipomi, "Viability of stretchable poly(3-heptylthiophene) (P3HpT) for organic solar cells and field-effect transistors," Synth. Met. **203**, 208–214 (2015).
[58]Y. D. Park, D. H. Kim, Y. Jang, J. H. Cho, M. Hwang, H. S. Lee, J. A. Lim, and K. Cho, "Effect of side chain length on molecular ordering and field-effect mobility in poly(3-alkylthiophene) transistors," Org. Electron. **7**, 514–520 (2006).
[59]J.-S. Kim, J.-H. Kim, W. Lee, H. Yu, H. J. Kim, I. Song, M. Shin, J. H. Oh, U. Jeong, T.-S. Kim *et al.*, "Tuning mechanical and optoelectrical properties of poly(3-hexylthiophene) through systematic regioregularity control," Macromolecules **48**, 4339–4346 (2015).
[60]H. Hoppe, D. A. M. Egbe, D. Muhlbacher, and N. S. Sariciftci, "Photovoltaic action of conjugated polymer/fullerene bulk heterojunction solar cells using novel PPE-PPV copolymers," J. Mater. Chem. **14**, 3462–3467 (2004).
[61]M. M. Wienk, M. Turbiez, J. Gilot, and R. A. J. Janssen, "Narrow-bandgap diketo-pyrrolo-pyrrole polymer solar cells: The effect of processing on the performance," Adv. Mater. **20**, 2556–2560 (2008).
[62]I. Kang, H.-J. Yun, D. S. Chung, S.-K. Kwon, and Y.-H. Kim, "Record high hole mobility in polymer semiconductors via side-chain engineering," J. Am. Chem. Soc. **135**, 14896–14899 (2013).
[63]G.-S. Ryu, K. H. Park, W.-T. Park, Y.-H. Kim, and Y.-Y. Noh, "High-performance diketopyrrolopyrrole-based organic field-effect transistors for flexible gas sensors," Org. Electron. **23**, 76–81 (2015).
[64]J.-R. Pouliot, B. Sun, M. Leduc, A. Najari, Y. Li, and M. Leclerc, "A high mobility DPP-based polymer obtained via direct (hetero)arylation polymerization," Polym. Chem. **6**, 278–282 (2015).
[65]A.-R. Han, G. K. Dutta, J. Lee, H. R. Lee, S. M. Lee, H. Ahn, T. J. Shin, J. H. Oh, and C. Yang, "ε-branched flexible side chain substituted diketopyrrolopyrrole-containing polymers designed for high hole and electron mobilities," Adv. Funct. Mater. **25**, 247–254 (2015).
[66]S. Savagatrup, D. Rodriquez, A. D. Printz, A. B. Sieval, J. C. Hummelen, and D. J. Lipomi, "[70]PCBM and incompletely separated grades of methanofullerenes produce bulk heterojunctions with increased robustness for ultra-flexible and stretchable electronics," Chem. Mater. **27**, 3902–3911 (2015).
[67]S. R. Dupont, M. Oliver, F. C. Krebs, and R. H. Dauskardt, "Interlayer adhesion in roll-to-roll processed flexible inverted polymer solar cells," Sol. Energy Mater. Sol. Cells **97**, 171–175 (2012).
[68]V. Brand, C. Bruner, and R. H. Dauskardt, "Cohesion and device reliability in organic bulk heterojunction photovoltaic cells," Sol. Energy Mater. Sol. Cells **99**, 182–189 (2012).
[69]L. Schmidt-Mende, A. Fechtenkotter, K. Mullen, E. Moons, R. H. Friend, and J. D. Mackenzie, "Self-organized discotic liquid crystals for

high-efficiency organic photovoltaics," Science (80-.) **293**, 1119–1122 (2001).
[70]X. Zhan, Z. Tan, B. Domercq, Z. An, X. Zhang, S. Barlow, Y. Li, D. Zhu, B. Kippelen, and S. R. Marder, "A high-mobility electron-transport polymer with broad absorption and its use in field-effect transistors and all-polymer solar cells," J. Am. Chem. Soc. **129**, 7246–7247 (2007).
[71]B. Friedel, C. R. McNeill, and N. C. Greenham, "Influence of alkyl side-chain length on the performance of poly(3-alkylthiophene)/polyfluorene all-polymer solar cells," Chem. Mater. **22**, 3389–3398 (2010).
[72]J. Choi, K.-H. Kim, H. Yu, C. Lee, H. Kang, I. Song, Y. Kim, J. H. Oh, and B. J. Kim, "Importance of electron transport ability in naphthalene diimide-based polymer acceptors for high-performance, additive-free all-polymer solar cells," Chem. Mater. **27**, 5230–5237 (2015).
[73]C. Guo, Y.-H. Lin, M. D. Witman, K. A. Smith, C. Wang, A. Hexemer, J. Strzalka, E. D. Gomez, and R. Verduzco, "Conjugated block copolymer photovoltaics with near 3% efficiency through microphase separation," Nano Lett. **13**, 2957–2963 (2013).
[74]V. Coropceanu, J. Cornil, D. A. da Silva Filho, Y. Olivier, R. Silbey, and J.-L. Bredas, "Charge transport in organic semiconductors," Chem. Rev. **107**, 926–952 (2007).
[75]R. Noriega, J. Rivnay, K. Vandewal, F. P. V. Koch, N. Stingelin, P. Smith, M. F. Toney, and A. Salleo, "A general relationship between disorder, aggregation and charge transport in conjugated polymers," Nat. Mater. **12**, 1038–1044 (2013).
[76]A. Salleo, R. J. Kline, D. M. DeLongchamp, and M. L. Chabinyc, "Microstructural characterization and charge transport in thin films of conjugated polymers," Adv. Mater. **22**, 3812–3838 (2010).
[77]M. Brinkmann, "Structure and morphology control in thin films of regioregular poly(3-hexylthiophene)," J. Polym. Sci., Part B: Polym. Phys. **49**, 1218–1233 (2011).
[78]T. M. Clarke and J. R. Durrant, "Charge photogeneration in organic solar cells," Chem. Rev. **110**, 6736–6767 (2010).
[79]S. A. Mollinger, B. A. Krajina, R. Noriega, A. Salleo, and A. J. Spakowitz, "Percolation, tie-molecules, and the microstructural determinants of charge transport in semicrystalline conjugated polymers," ACS Macro Lett. **4**, 708–712 (2015).
[80]F. C. Spano, "Modeling disorder in polymer aggregates: The optical spectroscopy of regioregular poly(3-hexylthiophene) thin films," J. Chem. Phys. **122**, 234701 (2005).
[81]A. Troisi, "The speed limit for sequential charge hopping in molecular materials," Org. Electron. **12**, 1988–1991 (2011).
[82]J. D. Roehling, K. J. Batenburg, F. B. Swain, A. J. Moulé, and I. Arslan, "Three-dimensional concentration mapping of organic blends," Adv. Funct. Mater. **23**, 2115–2122 (2013).
[83]H. Klauk, "Organic thin-film transistors," Chem. Soc. Rev. **39**, 2643–2666 (2010).
[84]L.-L. Chua, J. Zaumseil, J.-F. Chang, E. C.-W. Ou, P. K.-H. Ho, H. Sirringhaus, and R. H. Friend, "General observation of N-type field-effect behaviour in organic semiconductors," Nature **434**, 194–199 (2005).
[85]J. Zaumseil and H. Sirringhaus, "Electron and ambipolar transport in organic field-effect transistors," Chem. Rev. **107**, 1296–1323 (2007).
[86]G. Giri, E. Verploegen, S. C. B. Mannsfeld, S. Atahan-Evrenk, D. H. Kim, S. Y. Lee, H. A. Becerril, A. Aspuru-Guzik, M. F. Toney, and Z. Bao, "Tuning charge transport in solution-sheared organic semiconductors using lattice strain," Nature **480**, 504–508 (2011).
[87]C. J. Bettinger and Z. Bao, "Organic thin-film transistors fabricated on resorbable biomaterial substrates," Adv. Mater. **22**, 651–655 (2010).
[88]A. D. Printz, S. Savagatrup, D. Rodriquez, and D. J. Lipomi, "Role of molecular mixing on the stiffness of polymer:fullerene bulk heterojunction films," Sol. Energy Mater. Sol. Cells **134**, 64–72 (2015).
[89]C. Piliego and M. A. Loi, "Charge transfer state in highly efficient polymer–fullerene bulk heterojunction solar cells," J. Mater. Chem. **22**, 4141–4150 (2012).
[90]O. V. Mikhnenko, P. W. M. Blom, and T.-Q. Nguyen, "Exciton diffusion in organic semiconductors," Energy Environ. Sci. **8**, 1867–1888 (2015).
[91]Y. Liang, Z. Xu, J. Xia, S.-T. Tsai, Y. Wu, G. Li, C. Ray, and L. Yu, "For the bright future-bulk heterojunction polymer solar cells with power conversion efficiency of 7.4%," Adv. Mater. **22**, E135–E138 (2010).
[92]S. Wang, S. Fabiano, S. Himmelberger, S. Puzinas, X. Crispin, and A. Salleo, "Experimental evidence that short-range intermolecular aggregation is sufficient for efficient charge transport in conjugated polymers," Proc. Natl. Acad. Sci. U. S. A. **112**, 10599–10604 (2015).
[93]R. Street, J. Northrup, and A. Salleo, "Transport in polycrystalline polymer thin-film transistors," Phys. Rev. B **71**, 165202 (2005).
[94]J. Clark, C. Silva, R. Friend, and F. Spano, "Role of intermolecular coupling in the photophysics of disordered organic semiconductors: Aggregate emission in regioregular polythiophene," Phys. Rev. Lett. **98**, 206406 (2007).
[95]S. T. Turner, P. Pingel, R. Steyrleuthner, E. J. W. Crossland, S. Ludwigs, and D. Neher, "Quantitative analysis of bulk heterojunction films using linear absorption spectroscopy and solar cell performance," Adv. Funct. Mater. **21**, 4640–4652 (2011).
[96]A. D. Printz, A. S.-C. Chiang, S. Savagatrup, and D. J. Lipomi, "Fatigue in organic semiconductors: Spectroscopic evolution of microstructure due to cyclic loading in poly(3-heptylthiophene)," Synth. Met. **217**, 144–151 (2016).
[97]C. M. Stafford, B. D. Vogt, C. Harrison, D. Julthongpiput, and R. Huang, "Elastic moduli of ultrathin amorphous polymer films," Macromolecules **39**, 5095–5099 (2006).
[98]B. Gurmessa and A. B. Croll, "Influence of thin film confinement on surface plasticity in polystyrene and poly(2-vinylpyridine) homopolymer and block copolymer films," Macromolecules **48**, 5670–5676 (2015).
[99]C. M. Stafford, C. Harrison, K. L. Beers, A. Karim, E. J. Amis, M. R. VanLandingham, H.-C. Kim, W. Volksen, R. D. Miller, and E. E. Simonyi, "A buckling-based metrology for measuring the elastic moduli of polymeric thin films," Nat. Mater. **3**, 545–550 (2004).
[100]N. Lu, X. Wang, Z. Suo, and J. Vlassak, "Metal films on polymer substrates stretched beyond 50%," Appl. Phys. Lett. **91**, 221909 (2007).
[101]B. J. Gurmessa and A. B. Croll, "Onset of plasticity in thin polystyrene films," Phys. Rev. Lett. **110**, 074301 (2013).
[102]A. D. Printz, A. V. Zaretski, S. Savagatrup, A. S.-C. Chiang, and D. J. Lipomi, "Yield point of semiconducting polymer films on stretchable substrates determined by onset of buckling," ACS Appl. Mater. Interfaces **7**, 23257–23264 (2015).
[103]B. C.-K. Tee, C. Wang, R. Allen, and Z. Bao, "An electrically and mechanically self-healing composite with pressure- and flexion-sensitive properties for electronic skin applications," Nat. Nanotechnol. **7**, 825–832 (2012).
[104]M. Kaltenbrunner, T. Sekitani, J. Reeder, T. Yokota, K. Kuribara, T. Tokuhara, M. Drack, R. Schwödiauer, I. Graz, S. Bauer-Gogonea *et al.*, "An ultra-lightweight design for imperceptible plastic electronics," Nature **499**, 458–463 (2013).
[105]S. Savagatrup, E. Chan, S. M. Renteria-Garcia, A. D. Printz, A. V. Zaretski, T. F. O'Connor, D. Rodriquez, E. Valle, and D. J. Lipomi, "Plasticization of PEDOT:PSS by common additives for mechanically robust organic solar cells and wearable sensors," Adv. Funct. Mater. **25**, 427–436 (2015).
[106]H.-H. Chou, A. Nguyen, A. Chortos, J. W. F. To, C. Lu, J. Mei, T. Kurosawa, W.-G. Bae, J. B.-H. Tok, and Z. Bao, "A chameleon-inspired stretchable electronic skin with interactive colour changing controlled by tactile sensing," Nat. Commun. **6**, 8011 (2015).
[107]D. Ghezzi, M. R. Antognazza, R. Maccarone, S. Bellani, E. Lanzarini, N. Martino, M. Mete, G. Perile, S. Bisti, G. Lanzani *et al.*, "A polymer optoelectronic interface restores light sensitivity in blind rat retinas," Nat. Photonics **7**, 400–406 (2013).
[108]M. L. Hammock, A. Chortos, B. C.-K. Tee, J. B.-H. Tok, and Z. Bao, "25th anniversary article: The evolution of electronic skin (E-skin): A brief history, design considerations, and recent progress," Adv. Mater. **25**, 5997–6038 (2013).
[109]B. T. O'Connor, O. G. Reid, X. Zhang, R. J. Kline, L. J. Richter, D. J. Gundlach, D. M. Delongchamp, M. F. Toney, N. Kopidakis, and G. Rumbles, "Morphological origin of charge transport anisotropy in aligned polythiophene thin films," Adv. Funct. Mater. **24**, 3422–3431 (2014).
[110]R. H. Dauskardt, M. Lane, Q. Ma, and N. Krishna, "Adhesion and debonding of multi-layer thin film structures," Eng. Fract. Mech. **61**, 141–162 (1998).
[111]S. R. Dupont, E. Voroshazi, P. Heremans, and R. H. Dauskardt, "Adhesion properties of inverted polymer solarcells: Processing and film structure parameters," Org. Electron. **14**, 1262–1270 (2013).
[112]V. Brand, K. Levi, M. D. McGehee, and R. H. Dauskardt, "Film stresses and electrode buckling in organic solar cells," Sol. Energy Mater. Sol. Cells **103**, 80–85 (2012).
[113]N. R. Tummala, C. Bruner, C. Risko, J.-L. Bredas, and R. H. Dauskardt, "Molecular-scale understanding of cohesion and fracture in P3HT:fullerene blends," ACS Appl. Mater. Interfaces **7**, 9957–9964 (2015).
[114]C. Bruner and R. Dauskardt, "Role of molecular weight on the mechanical device properties of organic polymer solar cells," Macromolecules **47**, 1117–1121 (2014).

[115]C. Bruner, F. Novoa, S. Dupont, and R. Dauskardt, "Decohesion kinetics in polymer organic solar cells," ACS Appl. Mater. Interfaces **6**, 21474–21483 (2014).
[116]C. M. Stafford, S. Guo, C. Harrison, and M. Y. M. Chiang, "Combinatorial and high-throughput measurements of the modulus of thin polymer films," Rev. Sci. Instrum. **76**, 062207 (2005).
[117]J.-H. Lee, J. Y. Chung, and C. M. Stafford, "Effect of confinement on stiffness and fracture of thin amorphous polymer films," ACS Macro Lett. **1**, 122–126 (2012).
[118]A. D. Printz, S. Savagatrup, D. J. Burke, T. N. Purdy, and D. J. Lipomi, "Increased elasticity of a low-bandgap conjugated copolymer by random segmentation for mechanically robust solar cells," RSC Adv. **4**, 13635–13643 (2014).
[119]D. Tahk, H. H. Lee, and D.-Y. Khang, "Elastic moduli of organic electronic materials by the buckling method," Macromolecules **42**, 7079–7083 (2009).
[120]W. C. Oliver and G. M. Pharr, "An improved technique for determining hardness and elastic modulus using load and displacement sensing indentation experiments," J. Mater. Res. **7**, 1564–1583 (1992).
[121]K. Zeng, Z. K. Chen, L. Shen, and B. Liu, "Study of mechanical properties of light-emitting polymer films by nano-indentation technique," Thin Solid Films **477**, 111–118 (2005).
[122]M. R. VanLandingham, J. S. Villarrubia, W. F. Guthrie, and G. F. Meyers, "Nanoindentation of polymers: An overview," Macromol. Symp. **167**, 15–43 (2001).
[123]H. J. Kim, J. Kim, J. Ryu, Y. Kim, H. Kang, W. B. Lee, T. Kim, and B. J. Kim, "Architectural engineering of rod-coil compatibilizers for producing mechanically and thermally stable polymer solar cells," ACS Nano **8**, 10461–10470 (2014).
[124]T. Kim, J.-H. Kim, T. E. Kang, C. Lee, H. Kang, M. Shin, C. Wang, B. Ma, U. Jeong, T.-S. Kim *et al*., "Flexible, highly efficient all-polymer solar cells," Nat. Commun. **6**, 8547 (2015).
[125]I. Mcculloch, M. Heeney, C. Bailey, K. Genevicius, I. Macdonald, M. Shkunov, D. Sparrowe, S. Tierney, R. Wagner, W. Zhang *et al*., "Liquid-crystalline semiconducting polymers with high charge-carrier mobility," Nat. Mater. **5**, 328–333 (2006).
[126]R. Peng, B. Pang, D. Hu, M. Chen, G. Zhang, X. Wang, H. Lu, K. Cho, and L. Qiu, "An ABA triblock copolymer strategy for intrinsically stretchable semiconductors," J. Mater. Chem. C **3**, 3599–3606 (2015).
[127]J. K. Lee, W. L. Ma, C. J. Brabec, J. Yuen, J. S. Moon, J. Y. Kim, K. Lee, G. C. Bazan, and A. J. Heeger, "Processing additives for improved efficiency from bulk heterojunction solar cells," J. Am. Chem. Soc. **130**, 3619–3623 (2008).
[128]K. R. Graham, J. Mei, R. Stalder, J. W. Shim, H. Cheun, F. Steffy, F. So, B. Kippelen, and J. R. Reynolds, "Polydimethylsiloxane as a macromolecular additive for enhanced performance of molecular bulk heterojunction organic solar cells," ACS Appl. Mater. Interfaces **3**, 1210–1215 (2011).
[129]D. J. Lipomi, B. C.-K. Tee, M. Vosgueritchian, and Z. Bao, "Stretchable organic solar cells," Adv. Mater. **23**, 1771–1775 (2011).
[130]S. E. Root, S. Savagatrup, C. J. Pais, G. Arya, and D. J. Lipomi, "Predicting the mechanical properties of organic semiconductors using coarse-grained molecular dynamics simulations," Macromolecules **49**, 2886–2894 (2016).